UC Riverside
UC Riverside Previously Published Works

Title

Determining water quality requirements of coal seam gas produced water for sustainable irrigation

Permalink

https://escholarship.org/uc/item/7r1472pq

Authors

Mallants, Dirk
Šimůnek, Jirka
Torkzaban, Saeed

Peer reviewed
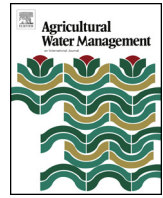
Determining water quality requirements of coal seam gas produced water for sustainable irrigation

Dirk Mallants [a,*], Jirka Šimůnek [b], Saeed Torkzaban [a]

[a] CSIRO Land and Water, Waite Road – Gate 4, Glen Osmond, SA 5064, Australia
[b] University of California, Riverside, CA 92521, USA

ABSTRACT

Coal seam gas production in Australia generates large volumes of produced water that is generally high in total dissolved solids and has a high sodium absorption ratio (SAR) which may affect soil structure, hydraulic conductivity, and crop production if used untreated for irrigation. By coupling major ion soil chemistry and unsaturated flow and plant water uptake, this study incorporates effects of salt concentrations on soil hydraulic properties and on root water uptake for soils irrigated with produced water featuring different water qualities. Simulations provided detailed results regarding chemical indicators of soil and plant health, i.e. SAR, EC and sodium concentrations. Results from a base scenario indicated that the use of untreated produced water for irrigation would cause SAR and EC values to significantly exceed the soil quality guide values in Australia and New Zealand (ANZECC). The simulations provided further useful insights in the type of coupled processes that might occur, and what the potential impacts could be on soil hydrology and crop growth. Calculations showed that the use of untreated produced water resulted in a decrease in soil hydraulic conductivity due to clay swelling causing water stagnation, additional plant-water stress and a reduction in plant transpiration. In case the produced water was mixed with surface water in a 1:3 ratio prior to irrigation, the calculated soil SAR values were much lower and generally acceptable for sandy to sandy-loam soil. The use of reverse osmosis treated produced water yielded an acceptable salinity profile not exceeding guide values for SAR and EC; the plant water stress was limited as there was no additional salinity stress associated with the low level of salts. Results further illustrated that accounting for coupled geochemical, hydrological and plant water uptake processes resulted in more accurate water balance calculations compared to an approach where such interactions were not implemented. Coupling unsaturated flow modelling with major ion chemistry solute transport using HYDRUS provides quantitative evidence to determine suitable water quality requirements for sustainable irrigation using coal seam gas produced water.

1. Introduction

Production of coal seam gas in Australia requires de-pressurisation of the coal seam layers by extracting large volumes of groundwater. Reducing the hydrostatic pressure on the gas in the pores of coal seams allows gas to flow through natural and enhanced fracture networks to the gas production well (Moore, 2012). Water extraction rates in the main coal seam gas areas in Australia vary over time and geographically (QWC, 2012). Based on a 50-year time frame that is generally assumed for forecast-ing water production (DNRM, 2012), average water production rates range from 0.028 GL/year in the Clarence Moreton basin (New South Wales) (RPS, 2011) to 75–98 GL/year in the Surat Basin (Queensland) (QWC, 2012). By 2050, most Australian coal seam gas areas will have reached the end of their production stage (DNRM, 2012).

Treated coal seam gas water may be utilised for beneficial uses, including agriculture (irrigation and stock), urban uses (town water supply) and industrial uses (construction and processing). Assessment of the beneficial use of treated coal seam gas water for the Central Condamine Alluvium (Queensland) indicates the region has the capacity to deliver 854 GL (gigalitres), or around 35% of the historic depletion, by 2050 to irrigators and the Chinchilla Weir water supply scheme (DNRM, 2013). Other irrigation projects in

Australia where produced water is used include large-scale forestry in Queensland's Bowen Basin and legume plantations (RPS, 2011). In the Bowen Basin, up to 8 ML/day of reverse osmosis (RO) treated produced water was used to irrigate 234 ha of pasture crop and an 800,000 tree timber plantation (Santos, 2009, 2010). Also in Queensland, 300 ha of oilseed-bearing legume tree (*Pongamia pinnata*) plantation are irrigated with RO treated produced water (Parsons, 2010).

Produced water is generally unsuitable for direct surface discharge or irrigation without any treatment or amendment (Stearns et al., 2005; Beletse et al., 2008; Nghiem et al., 2011). While sodium ions cause soil particles to disperse, particularly if the soils contain montmorillonite clays, most ions increase the aggregation of soil particles (Nghiem et al., 2011). Irrigation water with a high SAR[1] can lead to a decrease in infiltration and deterioration of the soil structure as the dispersed clay minerals, once dry, cause soils to become dense, cloddy and structureless, destroying natural particle aggregation. SAR values greater than 13 pose a risk to the soil ecosystem (Stearns et al., 2005), and even SAR values between 5 and 8 have been shown to cause irreversible plugging of soil pores and swelling (Mace and Amrhein, 2001). Traditional treatments to mitigate saline-sodic irrigation water can be used, such as for example the addition of gypsum and elemental sulphur (Vance et al., 2008; Šimůnek et al., 2006).

Studies have been undertaken to assess the feasibility of using sodium-rich produced water for salt-tolerant crop production (Johnston et al., 2008; Vance et al., 2008; Beletse et al., 2008). Vance et al. (2008) used saline-sodic coal seam gas produced water with an SAR between 17 and 57 for irrigating grasslands and hay-fields in the Powder River Basin, Wyoming. For the use of produced water to be effective, the method further required applications of gypsum and elemental S to provide calcium ions and an acidified soil environment to promote calcite dissolution. Further field studies in Wyoming with bioenergy feedstock species indicated that produced water can be used for short-period (2 years) irrigation of such crops (Burkhardt et al., 2015). However, the study also concluded that prolonged use of untreated produced water for irrigation would likely have deleterious long-term effects on the soil and plants unless the water was treated or diluted with good-quality water.

Water produced during the depressurisation phase of coal seam gas mining in Waterberg district, South Africa, is highly saline and dominated by sodium bicarbonate. With careful management, Beletse et al. (2008) determined that coal seam gas irrigation water with SAR values of 85 could be used to grow certain crops, but additions of gypsum and organic matter to the soil were necessary to counteract infiltration problems that arose due to the excessive sodium that had accumulated in the soil.

Investigations of soil and vegetation recovery in British Columbia document the natural recovery of salt-affected plots (Leskiw et al., 2012), with natural attenuation from above normal rainfall in the first few years after the salt deposition being effective in removing salts from the root zone and subsoil. These results, however, were obtained for a humid climate; it is expected that natural attenuation under arid or semi-arid climates would be much less effective. Bright and Addison (2002a,b) developed standardised guidelines to assist spill response and soil remediation in northern British Colombia at sites where salt-containing produced water is released as part of oil and gas exploration and extraction activities. Generic soil quality standards for human health, aquatic life, and soil ecological functioning, as manifested through soil invertebrate and plant responses, were developed for salt ions.

Whilst the impairment of metabolic functioning of soil microbes is recognised as playing a major role in nutrient cycling and other processes important to terrestrial ecosystems, there is insufficient data available to define a threshold for salt ions; instead, a microbial functional impairment standard is used that is developed from nutrient and energy cycling data.

In Australia, the Queensland Department of Environment and Heritage Protection (DEHP) recommends the minimum standards for using produced water for irrigation purposes. The guidelines indicate that the electrical conductivity (EC) should be less than 950 μS/cm or 0.95 dS/m (95th percentile over a one-year period), and the SAR should be less than 6 for heavy soils and less than 12 for light soils (95th percentile over a one-year period) (DEHP, 2014). Another potential issue when produced water is used for irrigation is the relatively high boron content. If not removed, boron can be damaging to some flora. The boron ANZECC guide value for long-term irrigation (up to 100 years) is 0.5 mg/L.

In Australia and New Zealand, the minimum quality of irrigation water is defined in The Australian and New Zealand Guidelines for Fresh and Marine Water Quality (ANZECC, 2000). Plant salt tolerances and recommended trigger values for metals and metalloids in irrigation water are also provided in ANZECC (2000). For instance, for different soil types, permissible levels of chloride, sodium, and SAR have been defined (Table 1).

To support the sustainable management of soil and landscapes under irrigated agriculture, Biggs et al. (2012) developed a framework to assess the salinity risk associated with the use of coal seam gas water for irrigation in the Queensland Murray-Darling Basin. Biggs et al. (2012) identified the description of the unsaturated zone as the key knowledge and data gap when conducting salinity risk assessments. In particular, studies are needed about (i) critical soil attributes (porosity, initial soil water content, substrate hydraulic conductivity) to depths below the "root zone", (ii) the extent of the root zone for different crops, and (iii) the quantification of lateral flow processes. Biggs et al. (2012) further highlighted the need to better define critical thresholds for agronomic and degradation purposes (e.g. acceptable root zone salinity) across landscapes, improve process understanding such as the fate of excess water (lateral flow or drainage), and deeper soil/regolith processes and properties.

The current study endeavours to address those knowledge gaps that relate to better process understanding (e.g., critical soil properties, critical thresholds) using the unique features of the HYDRUS-1D simulator that are relevant for salinity risk assessment (Jacques et al., 2013a; Šimůnek et al., 2006, 2016). To this end, this study simulates coupled processes of variably saturated water flow, plant water uptake and coupled transport of multiple major ions in soils irrigated with produced water of different water qualities. Through this process coupling, we explicitly include critical soil processes required for salinity risk assessment associated with coal seam gas produced water in the analysis. Simulations of the movement of multiple ions in a vegetated soil profile under irrigation are based on the major ion chemistry module UnsatChem (Šimůnek and Suarez, 1994) implemented in the finite element code HYDRUS-1D (Šimůnek et al., 2008).

2. Materials and methods

2.1. Soil hydrological model

Simulation of variably saturated flow in soil requires a mathematical relationship between (i) the soil water content (θ) and the soil pressure head (h), i.e. the soil water retention curve $\theta(h)$, and (ii) either the water content or the pressure head and the unsaturated hydraulic conductivity $K(\theta)$ and $K(h)$, respectively. We applied the

---

[1] Sodium adsorption ratio (SAR) = $[Na^+]/\{([Ca^{2+}]+[Mg^{2+}])/2\}^{1/2}$ where $[Na^+]$, $[Ca^{2+}]$, and $[Mg^{2+}]$ are in meq/L.

Table 1
Permissible levels of irrigation water quality parameters to preserve soil and plant health.

Parameter	Maximum (DEHP, 2014)	ANZECC (2000)
Electrical conductivity (μS/cm)[k]	<950[i]	<650
SAR	<6[i] for heavy soils; <12[i] for light soils	>20[a]; 20–8[b]; 13–6[c]; 11–5[d]
Bicarbonate (mg/L)	100[j]	No trigger value recommended
Fluoride (mg/L)	2	1
pH	6–8.5[i]	6–9
Chloride (mg/L)		<175[e]; 175–350[f]; 350–700[g]; > 700[h]
Sodium (mg/L)		<115[e]; 115–230[f]; 230–460[g]; >460[h]
Heavy metals and metalloids (trigger values in mg/L; short-term use up to 20 years)	Al (20); As (2); Cd (0.05); Cr (1); Co (0.1); Cu (5); Fe (10); Li (2.5); Pb (5); Mn (10); Hg (0.002); Mb (0.05); Ni (2); Zn (5)	

[a] Sand-sandy loam.
[b] Loam-silty loam.
[c] Clay loam.
[d] Light clay.
[e] Sensitive crop.
[f] Moderately sensitive crop.
[g] Moderately tolerant crop.
[h] Tolerant crop.
[i] 95th percentile over a one-year period.
[j] DERM (2010).
[k] 1000 μS/cm = 1 dS/m.

analytical model of van Genuchten, i.e., nonhysteretic, to describe the soil water retention curve, $\theta(h)$ (van Genuchten, 1980), since it permits a relatively good description of $\theta(h)$ for many soils using only a limited number of parameters. The van Genuchten soil moisture retention characteristic is defined as:

$$\theta(h) = \theta_r + \frac{\theta_s - \theta_r}{(1 + |ah|^n)^m} \tag{1}$$

where θ_r is the residual water content [cm^3/cm^3], θ_s is the saturated water content [cm^3/cm^3], and α [1/m], n [–] and m (=1 – 1/n) [–] are the retention curve shape parameters. The van Genuchten (1980) $\theta(h)$ equation has the additional advantage that when coupled with the unsaturated hydraulic conductivity $K(h)$ model of Mualem (1976), it produces the following closed-form expression:

$$K(h) = K_s S_e^l [1 - (1 - S_e^{1/m})^m]^2 \tag{2}$$

where K_s is saturated hydraulic conductivity [cm/day], $S_e = (\theta - \theta_r)/(\theta_s - \theta_r)$ is the effective saturation [–], $m = 1 - 1/n$, and $n > 1$. The pore-connectivity parameter (l) was estimated by Mualem (1976) to be about 0.5 as an average for many soils. In this study, we use Eq. (2) with the l parameter fixed at 0.5.

2.2. Soil geochemical model

Migration of chemicals in soil is primarily by advection and dispersion (ignoring gaseous transport) when advection is greater than the rate of diffusion. For the transport of contaminants during transient water flow, HYDRUS implements the advection–dispersion equation (Šimůnek et al., 2008). In this study, a dispersivity of 0.1 m was taken, or one tenth of the total travel distance from top to bottom of the 1-m deep soil profile.

The solute transport module of HYDRUS-1D as described above is limited to single ions, or ions subject to relatively simple first-order consecutive decay or transformation reactions (e.g., nitrification–denitrification chains, or radionuclide decay chains). As an extension to this approach, HYDRUS-1D implements a major ion chemistry module based on the UnsatChem model (Šimůnek and Suarez, 1994, 1997; Šimůnek et al., 2008). The UnsatChem module of HYDRUS-1D enables quantitative predictions of processes involving major ions, such as simulations of the effects of salinity on plant growth and estimating the amount of water and amendments required to reclaim soil profiles to desired levels of salinity and ESP (exchangeable sodium percentage) (Šimůnek et al., 2006).

The UnsatChem module (Šimůnek and Suarez, 1994) considers the transport of major ions and carbon dioxide in soils. The major variables of the chemical system are Ca, Mg, Na, K, SO$_4$, Cl, NO$_3$, H$_4$SiO$_4$, alkalinity, and CO$_2$ (Supplementary Material Table S1). The model accounts for equilibrium chemical reactions between these components such as complexation, cation exchange, and precipitation–dissolution. For the precipitation–dissolution of calcite and the dissolution of dolomite, either equilibrium or multicomponent kinetic expressions are used, including both forward and backward reactions. Other precipitation–dissolution reactions considered involve gypsum (CaSO$_4$·2H$_2$O), hydromagnesite (Mg$_5$(CO$_3$)$_4$(OH)$_2$·4H$_2$O), nesquehonite (MgCO$_3$·3H$_2$O) (Mg), and sepiolite (Mg$_2$Si$_3$O$_{7.5}$(OH)·3H$_2$O). Since the ionic strength of soil solutions can vary considerably in time and space and often reach high values, both the modified Debye–Hückel and Pitzer expressions were incorporated into the model, thus providing options for calculating single-ion activities (Šimůnek et al., 2013).

Partitioning of dissolved major ions between the solid and solution phases is described with the Gapon equation (White and Zelazny, 1986) provided in the major ion chemistry module. This requires the definition of the Gapon Exchange Constants for exchange of calcium and magnesium, calcium and potassium, and calcium and sodium. The Gapon Exchange Constants are taken from Jacques et al. (2012) and are interpreted as follows: for the Ca^{2+}/Mg^{2+} exchange ($K_{Ca/Mg}$ = 1.2), Ca^{2+} is the preferred ion relative to Mg^{2+} on the exchange complex. For the Ca^{2+}/Na$^+$ exchange ($K_{Ca/Na}$ = 2.9), Ca^{2+} is the preferred ion relative to Na$^+$. Finally, for the Ca^{2+}/K$^+$ exchange ($K_{Ca/K}$ = 0.2), K$^+$ is the preferred ion relative to Ca^{2+}.

UnsatChem also considers the effects of solution composition on the unsaturated soil hydraulic properties. The accumulation of monovalent cations, such as sodium and potassium, often leads to clay dispersion, swelling, flocculation and overall poor soil physico-mechanical properties. These processes have an adverse effect on the soil hydraulic properties including hydraulic conductivity, infiltration rates and soil water retention as a result of swelling and clay dispersion. These negative effects are usually explained based on the diffuse double layer theory.

The effect of solution chemistry on the hydraulic conductivity in the major ion chemistry module is calculated as:

$$K(h, pH, SAR, C_0) = r(pH, SAR, C_0)K(h) \tag{3}$$

where SAR is the sodium adsorption ratio, C_0 is the total salt concentration of the ambient solution (meq/L), and r is a scaling factor

which represents the effect of the solution composition on the final hydraulic conductivity [–], and which is related to pH, SAR, and salinity (Šimůnek et al., 2008). Conceptually, this effect is related to clay swelling as a result of changes in ion composition here expressed via the parameters SAR and C_0 (McNeal, 1968, 1974). Although soil water retention curves may also be affected by SAR and electrolyte concentrations (e.g., Lenhard and Brooks, 1986), this is not being considered in the current simulations.

We note that other effects of solution chemistry on hydraulic properties such as mineral precipitation resulting in a decrease of pore space and hence a decrease in hydraulic conductivity may be equally important to determine a soil's water balance under irrigation in arid and semi-arid regions. Examples of a more general approach to couple major ion chemistry with porous media hydraulic and solute transport parameters are available from Jacques et al. (2013a,b).

2.3. Soil hydrological data

The soil profile used in this study was assumed to be 1 m deep, with three soil layers: 0–0.3 m, 0.3–0.7 m, and 0.7–1.0 m. The van Genuchten soil hydraulic properties were taken from Bennett (2012). These soil hydraulic properties were calculated on the basis of the pedotransfer functions of Minasny and McBratney (2002) using soil data points within the Cox's Creek catchment, New South Wales. For three soil horizons, the particle size distribution and the bulk density from the SALIS (New South Wales Soil And Land Information System) dataset were used as predictor variables in the pedotransfer functions. From six soil types (Tenosols, Dermosols, Vertosols, Chromosols, Sodosols, Kandosols), Vertosols were most prominent in 84 out of 143 soil profiles (59%). Vertosol hydraulic properties were therefore selected here for the simulations (Supplementary Material Table S2). The mean soil water retention curves together with their uncertainty bands (mean ± 2 standard deviations) are shown in Supplementary Material Figure S1.

In order to reach the (pseudo) steady-state concentrations profile, the following hypothetical irrigation scheme was used. The potential ET is equal to 1 cm/day (based on the average from January 2014 in Narrabri, BOM, 2014), and is divided into potential evaporation (2 mm/day) and potential transpiration (8 mm/day). Over a 5-day period 6 cm of irrigation was applied on the first day followed by 4 days of not irrigating; this resulted in a total of 73 irrigation days out of a simulation period of 365 days. For each 5-day period, this yielded an irrigation excess of 20% above the potential ET for each day. The annual total irrigation of 438 cm is much higher than the combined rainfall and irrigation in irrigation areas of the Northern Darling Basin for crops such as cotton (up to nearly 140 cm) or sorghum (up to 110 cm) (Silburn and Montgomery, 2004). However, irrigation of pasture, especially for grazing (beef and lamb), uses more water: for example, nearly 150 cm was recorded in a flood irrigated pasture in the South East of South Australia (Horizon, 2006). The application rate used in this study, therefore, corresponds to the equivalent applied water of two to three growing seasons. Our purpose was not to have the most realistic irrigation regime, rather, we applied a simplified water application rate that would simplify the analysis of the complex coupled chemical-hydrological processes.

Zero precipitation was considered for the modelling; while this is a simplification of a soil's hydrological balance and does not account for effects of rainfall salinity on the salt mass balance, it does allow to focus on effects of irrigation only when coupled chemical-hydrological-biological processes are considered. The root zone was assumed to be 0.50 m deep and root distribution was assumed to decrease linearly with depth. The initial pressure head at the beginning of each simulation was assumed

to be -1 m throughout the soil profile. The top boundary condition was specified as an atmospheric boundary with surface runoff, i.e. whenever rainfall intensity exceeds the soil's infiltration capacity ponding does not occur and all excess water is considered runoff and removed from the soil surface. At the bottom of the profile, a free drainage BC was imposed. The soil water and chemical mass balances were calculated for one year.

2.4. Crop data

Two cases were considered to simulate stress effects: (i) water stress without salinity stress and (ii) both water and salinity stresses on crop production. First, the effect of water stress was separately analysed using the Feddes' model (Feddes et al., 1978). A conceptual representation of the suction-dependent plant-water stress response function is shown in Supplementary Material Figure S2 and relevant parameters based on Wesseling et al. (1991) in Table S3.

When salinity stress is considered in HYDRUS, a selection must be made whether the effect of salinity stress is additive or multiplicative to water stress. Here the multiplicative Threshold Model according to Maas (1990) was selected. The Threshold Model has two parameters, the threshold parameter and the slope parameter (Table S3). The first parameter represents the value of the minimum osmotic head (the salinity threshold) above which root water uptake occurs without any reduction. The second parameter is the slope of the curve determining the fractional root water uptake decline per unit increase in salinity below the threshold. Root water uptake reduction parameters for alfalfa were used to investigate combined water and salinity stress as no salinity stress parameters are available for pasture (all other root water uptake parameters are those for pasture).

The volume of water removed from a unit volume of soil per unit time due to plant water uptake, S(h) [day^{-1}], is defined as (Šimůnek et al., 2008)

$$S(h) = \alpha(h)b(z)T_{\mathrm{p}} \tag{4}$$

where $\alpha(h)$ is the plant-water stress response function (between 0 and 1, see Supplementary Material Figure S2), $b(z)$ is the normalised water uptake distribution [cm^{-1}] (here assumed linearly decreasing with depth), and T_{p} is potential transpiration [cm/day]. With $T_{\mathrm{p}} = 0.8$ cm/day, and $b(z=0) = 0.04$ cm^{-1} (when rooting depth = 50 cm; $2 \times 1/50$), $S(h)$ at the soil surface equals 0.032 day^{-1}.

2.5. Chemical composition of irrigation water

Three different chemical compositions of irrigation water were assumed (Table 2); the first corresponds to untreated produced water, the second is a 3:1 surface-water amended produced water, and the third is RO-treated produced water. The first (untreated) and third (treated) compositions represent end-members that can be mixed to various degrees to obtain fit-for-purpose irrigation water. Unlike the amended and treated produced waters that are actually being field-tested and/or being used in commercial irrigation schemes, the untreated produced water would almost certainly not receive any permission for use as irrigation water owing to its high potassium and SAR values (Table 2). It is included here only to demonstrate effects of several interacting processes, such as major ion composition triggering a reduction in soil hydraulic conductivity and subsequent modification of water redistribution in the soil profile and how root water uptake responds to such changes. It is worth noting that the treated water is still much more saline than rainfall. In other words, even irrigation with treated produced water is likely to have some effect on the soil's chemical balance.

Table 2
Composition of untreated, amended, and treated produced waters from Australian coal basins. Treated/rain water = ratio of treated produced water to rain water composition.

	Alkalinity	Cl	SO$_4$	Ca	K	Mg	Na	SAR
Untreated produced water								
mg/L	1706	593	22.8	10.4	5.6	8.9	1406	
meq/L	41.9	16.7	0.47	0.52	0.14	0.74	61.1	77
EC$_i$[a] (µS/cm)	1245	1278	38	31	11	39	3064	Total EC = 5705
%EC$_i$[a]	21.8	22.4	0.7	0.5	0.2	0.7	53.7	100%
Amended produced water (3:1 ratio surface water:produced water)								
mg/L	183	164	337	10.30	34.8	6.5	184	
meq/L	4.5	4.6	7.0	0.51	0.89	0.53	8.0	11
EC$_i$[a] (µS/cm)	134	353	561	31	65	28	401	Total EC = 1573
%EC$_i$[a]	8.5	22.5	35.7	1.9	4.2	1.8	25.5	100%
Treated produced water								
mg/L	25	67	1	10.33	0.43	7.6	28.7	
meq/L	0.61	1.89	0.02	0.52	0.011	0.62	1.25	1.6
EC$_i$[a] (µS/cm)	18.2	144.3	1.67	30.7	0.81	33	62.5	Total EC = 291
%EC$_i$[a]	6.3	49.6	0.6	10.5	0.3	11.3	21.5	100%
Treated/rain water	417	103	3	43	4	95	60	
Electrical conductivity for ions as trace concentration in water at 25 °C								
S cm^2/mol	44.5	76.35	160	119	73.5	106	50.1	

[a] The electrical conductivity contribution of each ion (%EC$_i$) to the total EC of the solution is calculated as (Appelo and Postma, 2004):

Table 3
Initial concentrations of exchangeable cations (*Source*: Ringrose-Voase, 2004) and initial solution composition used to calculate initial solution in equilibrium with the cation exchange complex. Data represents composition of rainwater in Wagga-Wagga (*Source*: Crosbie et al., 2012). Gapon Exchange Constants (*Source*: Jacques et al., 2012).

Soil layer	CEC (meq/kg soil)	Gapon Exchange Constants		
		K [Ca/Mg]	K [Ca/Na]	K [Ca/K]
1 (0–0.3 m)	275	1.2	2.9	0.2
2 (0.3–0.7 m)	278	1.2	2.9	0.2
3 (0.7–1.0 m)	274	1.2	2.9	0.2

Exchangeable cations for layer 1

Ions	Ca	Mg	Na	K
mmol/kg	86.3	44	4.6	9.4
meq/kg	173	88	4.6	9.4

Initial solution composition (meq/L)

Ca	Mg	Na	K	Alkalinity	SO$_4$	Cl
0.012	0.0066	0.021	0.0028	0.00098	0.0069	0.018

It is important to note that from all the ions considered in the simulation, only potassium (K) has an ANZECC guide value for irrigation (ANZECC, 2000). For long-term use (up to 100 years), the guide value for K is 0.05 mg/L. For short term use (up to 20 years), the guide value is 0.8 mg/L. The calculated SAR for the untreated produced water is 77 (Table 2); this is considerably higher than the DEHP maximum guide value of 12 for light soils (95th percentile over a one-year period) (DEHP, 2014).

2.6. Initial soil chemical composition

The initial concentrations of soil exchangeable cations (Table 3) were taken from a lysimeter study by Ringrose-Voase (2004). The lysimeter is located in paddock C1 at the Australian Cotton Research Institute (ACRI) near Narrabri in northern New South Wales (30°11.53′ South, 149°36.31′ East). The soil is a Haplic, self-mulching, Grey Vertosol. The bulk density for different soil depths was estimated to range between 1.32 and 1.45 g/cm^3 (Ringrose-Voase, 2004). Because the total cation exchange capacity is similar for all three soil layers, the cation exchange capacity and the concentration of exchangeable cations of the first layer was assigned to all three layers.

The initial solution composition in the soil profile (Table 3) was defined using the solution composition of rainwater measured in Wagga-Wagga (Crosbie et al., 2012). Note that this solution will be automatically brought into equilibrium with the cation exchange complex.

2.7. Simulation scenarios

Scenario 1: A base scenario against which other scenarios can be compared. The base scenario involves soil water balance and general solute transport calculations without (i) effects of major ion chemistry on hydraulic properties, (ii) effects of salinity stress on root water uptake, and (iii) effects of competing adsorption between major ions on ion migration in soil. Root water uptake without solute stress is calculated for pasture and alfalfa. The irrigation water is solute-free and only contains a single tracer, assuming a hypothetical unit tracer concentration of 1 mg/L, used to evaluate solute migration based on a 6/5 cm/day irrigation rate (averaged across one day of irrigation at 6 cm/day followed by 4 days of zero irrigation). The standard Hydrus "General Solute Transport" module was used to model salinity as a non-reactive tracer with a unit input concentration.

Scenario 2: Water balance calculations account for root water uptake with a multiplicative solute stress. Major ion chemistry solute transport is invoked excluding the effects of a reduction in hydraulic conductivity. This scenario uses untreated produced water at a 6 cm/day irrigation rate (for chemical composition see Table 3). This scenario uses the Hydrus "Major Ion Chemistry" (UnsatChem) module to calculate concentrations of major ions (Ca, Mg, Na, K, alkalinity, Cl, SO$_4$) present in irrigation water.

Scenario 3: The main difference with Scenario 2 is that major ion chemistry solute transport now includes calculation of reduction in hydraulic conductivity due to soil solution chemistry (based on Eq. (3)). Untreated produced water is used at a lower 4 cm/day irrigation rate followed by 4 days of no irrigation to avoid water ponding due to reduced hydraulic conductivity (calculations with 6 cm/day irrigation rate produced ponding, results not shown). In addition to the processes considered in Scenario 2, the reduction of hydraulic conductivity due to the solution composition is accounted for (McNeal, 1968, 1974). Scenario 4: Same as Scenario 3, but now surface water-amended produced water (at a 3:1 surface water:produced water ratio) is used at a 6 cm/day irrigation rate (for chemical composition see Table 2).
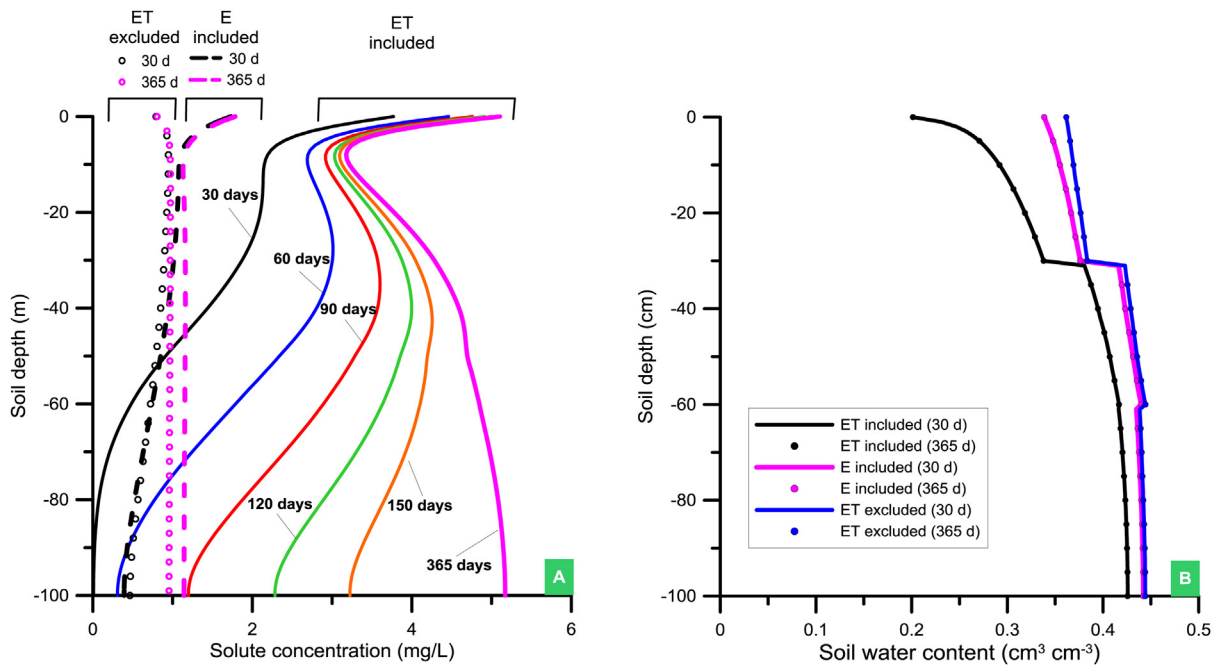
Fig. 1. (A) Simulated solute concentrations following infiltration of solute-containing irrigation water (Scenario 1). Comparison of models including ET (solid lines), including E only (evaporation, dashed lines) or excluding ET (evapotranspiration, symbols). (B) Comparison of simulated soil water contents for models including ET, excluding T, or excluding ET.

Scenario 5: Same as Scenario 4, but here treated produced water is used at a 6 cm/day irrigation rate (for chemical composition see Table 2).

3. Results and discussion

3.1. Base scenario simulation

Simulated water content and pressure head for the base scenario (Supplementary Material Figure S3) time series show typical patterns linked to alternating periods of soil wetting during and following irrigation and drying periods in the intermittent periods between irrigation events. At deeper depths in the soil profile, the variations become smaller as the water redistribution becomes increasingly buffered as it moves through the soil.

The solute accumulation in the soil profile at different depths is shown in Fig. 1A. Three different simulation results are shown to illustrate the effect evaporation and transpiration processes have on solute concentration.

First, consider the solute concentration profiles at increasing times since the start of the irrigation for simulations that include evaporation and transpiration (Fig. 1A). Profiles are obtained at the end of each irrigation-free four-day period, just before irrigation starts (see output time steps on Supplementary Material Figure S2). During this four-day period, as a result of evaporation, water content at the soil surface decreases (Fig. 1B), creating an upward pressure head gradient, which produces upward water flow towards the soil surface. Water flowing towards the soil surface carries with it solute ions, which accumulate at the soil surface during evaporation. Note that during evaporation, water leaves the soil surface while leaving solute ions behind. As a result of decreasing water contents and upward water flow towards the surface (bringing additional solute ions), the concentration of solute ions increases significantly during this time period (visible in the top 0.1 m of the soil profile, Fig. 1A). Transpiration will further reduce the water content across the root zone (Fig. 1B), which further increases solute concentrations.

As a whole, the solute profiles reflect the equilibrium between infiltration with irrigation water, water and solute redistribution due to transpiration and evaporation, and downward leaching (Fig. 1A). The prominent effects of transpiration and evaporation on the solute profile become further apparent when these processes are suppressed (Fig. 1A). For instance, when transpiration T is suppressed during the simulations a much smaller solute concentrations across the entire soil profile become apparent. If subsequently also soil evaporation E is suppressed, the effect is mainly a further concentration reduction near the soil surface while deeper in the soil the profiles that exclude T and ET (soil evaporation and plant transpiration) are similar at 30 days and only slightly different at 365 days. These effects are mainly caused by differences in soil water contents between the different models (with or without T and ET): the highest water content is observed when both transpiration and evaporation are suppressed, whereas the lowest water contents exist when those processes are included (Fig. 1B). As noted, the effect of suppressing transpiration is much greater than suppressing evaporation (daily potential transpiration rate is 0.8 cm/day while daily potential evaporation rate is 0.2 cm/day). At the top of the soil profile, the water content without ET is 1.7 times larger than when ET is included. This ratio is close to the ratio of 2.2 obtained by dividing solute concentration with ET and without ET at the same depth.

Cumulative water fluxes across model boundaries (soil surface and bottom of the model domain) were calculated for pasture and alfalfa (note that only the water stress response function is applied for both crops). As can be observed from Fig. 2A and Table 4, there is no noticeable difference between the two crops. For both crops, the potential (292 cm) and actual (281 cm) annual cumulative transpiration fluxes are very similar, indicating there was little water stress during the simulations. The cumulative potential and actual surface fluxes (considering infiltration and evaporation) are both negative (downward) and identical (−365 cm), meaning potential and actual evaporation are equal (73 cm). The surface flux is based on an annual total irrigation of −438 cm (negative in the water balance calculation). The cumulative actual bottom flux (i.e. drainage)
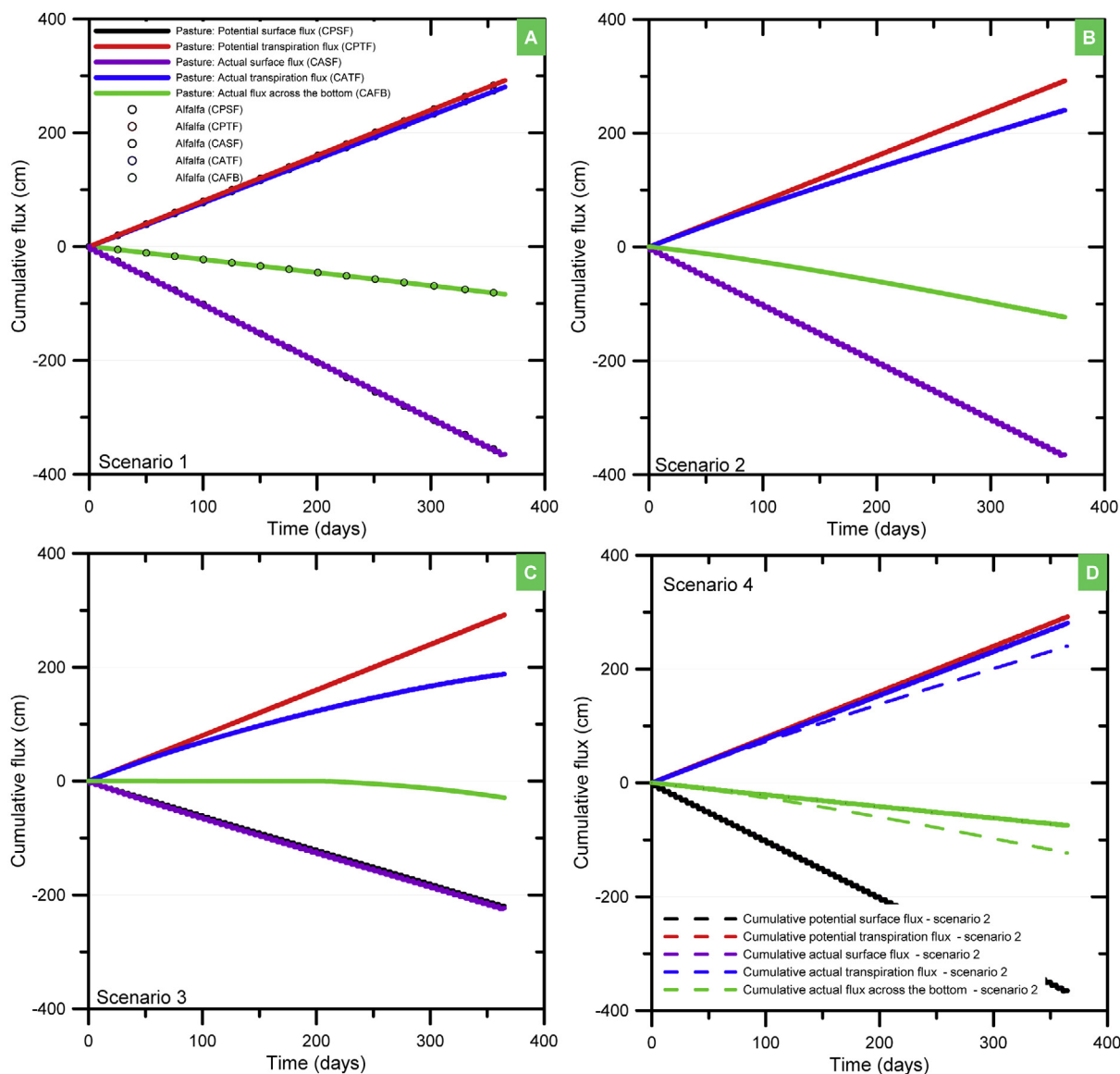
Fig. 2. Cumulative potential (black) and actual (purple) surface fluxes (infiltration minus evaporation), cumulative potential (red) and actual (blue) transpiration fluxes, and cumulative actual (green) bottom flux. Cumulative potential and actual surface fluxes are identical across all scenarios. (A) Scenario 1 (pasture and alfalfa). (B) Scenario 2 (pasture). (C) Scenario 3 (pasture). (D) Scenario 4 (pasture). (For interpretation of the references to color in this figure legend, the reader is referred to the web version of the article.)

Table 4
Water balance components for a 365 day simulation period. Negative infiltration values means inflow; negative net drainage values means outflow.

Scenario	Cumulative infiltration (cm)	Cumulative actual transpiration (cm)	Cumulative actual evaporation (cm)	Cumulative net drainage (cm)
1: Pasture – tracer only–ADE	−438[a]	281 [96%]	73 [100%]	−84
1: Alfalfa – tracer only–ADE	−438[a]	281 [96%]	73 [100%]	−83
2: Pasture – UPW–MIC–WSS	−438[a]	240 [82%]	73 [100%]	−123
3: Pasture – UPW–MIC–WSS–KRM	−292[b]	188 [64%]	69 [95%]	−29
4: Pasture – SAPW–MIC–WSS–KRM	−438[a]	281 [96%]	73 [100%]	−84
5: Pasture – TPW–MIC–WSS–KRM	−438[a]	280 [96%]	73 [100%]	−84

ADE: standard advection–dispersion model; UPW: untreated produced water; MIC: major ion chemistry combined with ADE; WSS: water and solute stress model; KRM: hydraulic conductivity reduction model; SAPW: surface water amended produced water; TPW: treated produced water.

[a] 0.06 cm/day once every 5 days.
[b] 0.04 cm/day once every 5 days.

is negative, i.e. −84 cm for pasture and −83 cm for alfalfa. This drainage flux is expected as the irrigation rate exceeds the potential ET by a factor of 6 during day one of the irrigation cycle (6 cm irrigation with 1 cm potential ET).

3.2. Major ion chemistry

We now consider major ion chemistry to simulate behaviour of multiple solutes added to the soil profile through the use of pro-
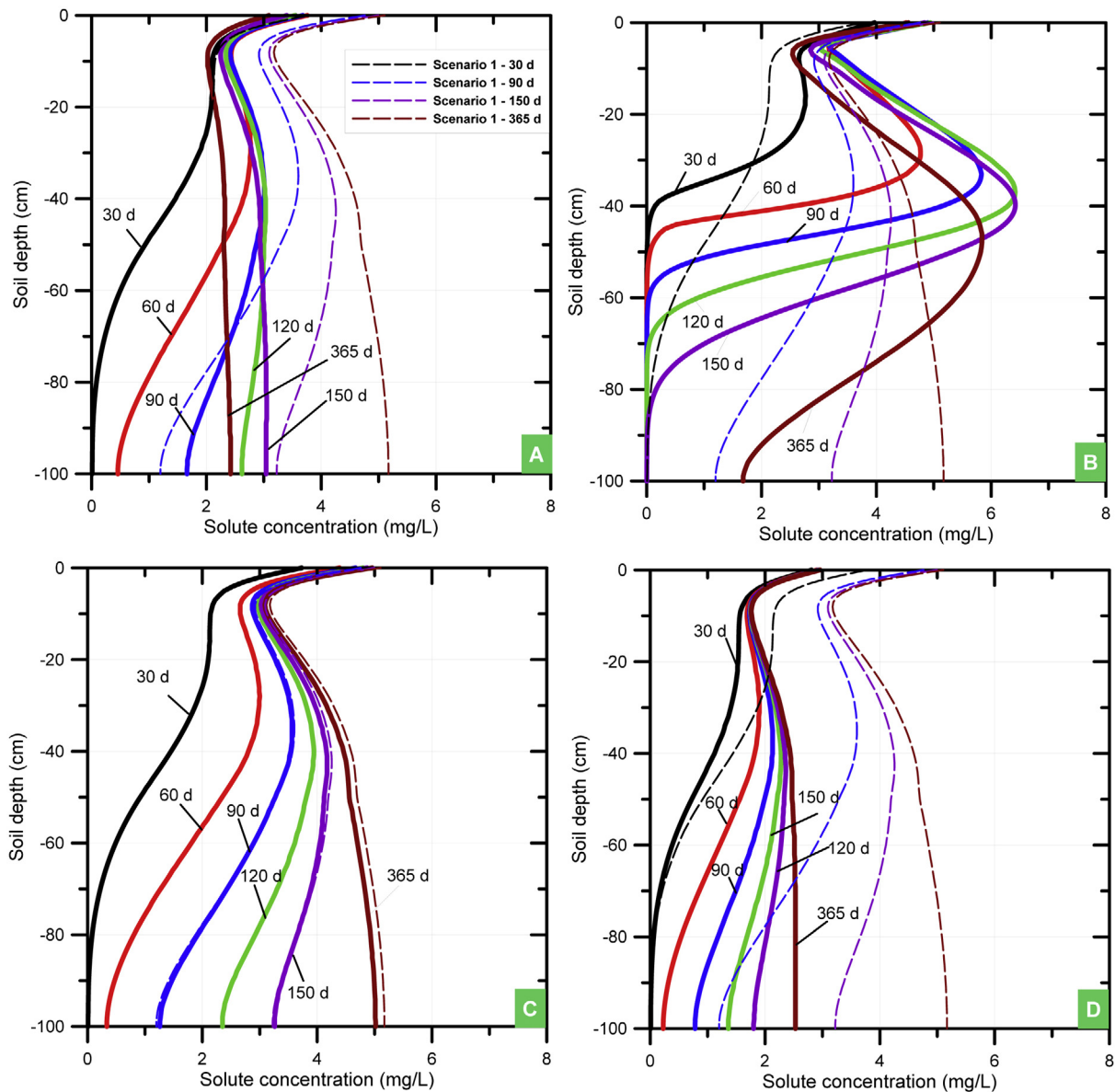
Fig. 3. Solute tracer concentration profiles for Scenarios 2 (A), 3 (B), 4 (C) and 5 (D). Dashed lines show corresponding solute tracer concentration profiles for Scenario 1.

duced water; Scenario 2 with untreated water is discussed first. This scenario provides insight into the distribution of individual ions (both in the aqueous phase and adsorbed on the solid phase), the EC and the SAR in soil. The simulations also provide concentrations of any minerals such as calcite, dolomite or gypsum, should they form (see Supplementary Material Table S1 for a full list of minerals simulated). Scenario 2 further links the soil chemistry (i.e. salinity) to the salinity stress of plants (in addition to the water stress invoked in Scenario 1), allowing for calculations of the reduction in water uptake by vegetation due to differences in water quality. The reduction in water uptake, in turn, has an effect on the water and solute distribution in the soil profile, and thus on the drainage flux of water and solutes across the bottom of the profile. Unlike Scenarios 3, 4, and 5, the effects of salinity on hydraulic properties were not considered in Scenario 2.

Due to the combined effects of water and salinity stresses on root water uptake, which will be explained in the following paragraph, actual transpiration for Scenario 2 (240 cm) is considerably lower than potential transpiration (292 cm) (Fig. 2 and Table 4). Lower transpiration results in more water remaining in the soil (Fig. 4A),

and more water draining through the bottom of the profile (123 cm for Scenario 2 versus 84 cm for Scenario 1, Table 4).

The tracer profile developed over one-year simulation for Scenario 2 is quite different from Scenario 1 (Fig. 3A). If only water stress is accounted for in the absence of major ion chemistry (Scenario 1), the tracer concentration gradually builds up over the entire soil profile, with a sharp concentration gradient near the soil surface (Fig. 3A). Also note that the output is obtained just before irrigation starts (at the end of a period with irrigation at day 1 followed by 4 days of ET), when water contents in the top layer are lowest (and consequently concentration are the highest). When major ion chemistry and the salinity stress are accounted for (Scenario 2), the salinity stress results in a significant reduction in the root water uptake and hence a reduction in actual transpiration, i.e. from 281 (Scenario 1) to 240 cm (Fig. 2B). This, in turn, mainly changes the solute concentration distributions whereas water content is less impacted as exemplified in Figs. 3A and 4A, respectively: the lower concentrations in the bottom part of the soil profile are due to the higher drainage flux (−123 cm for Scenario 2 compared to −84 cm for Scenario 1) causing dilution of the tracer.
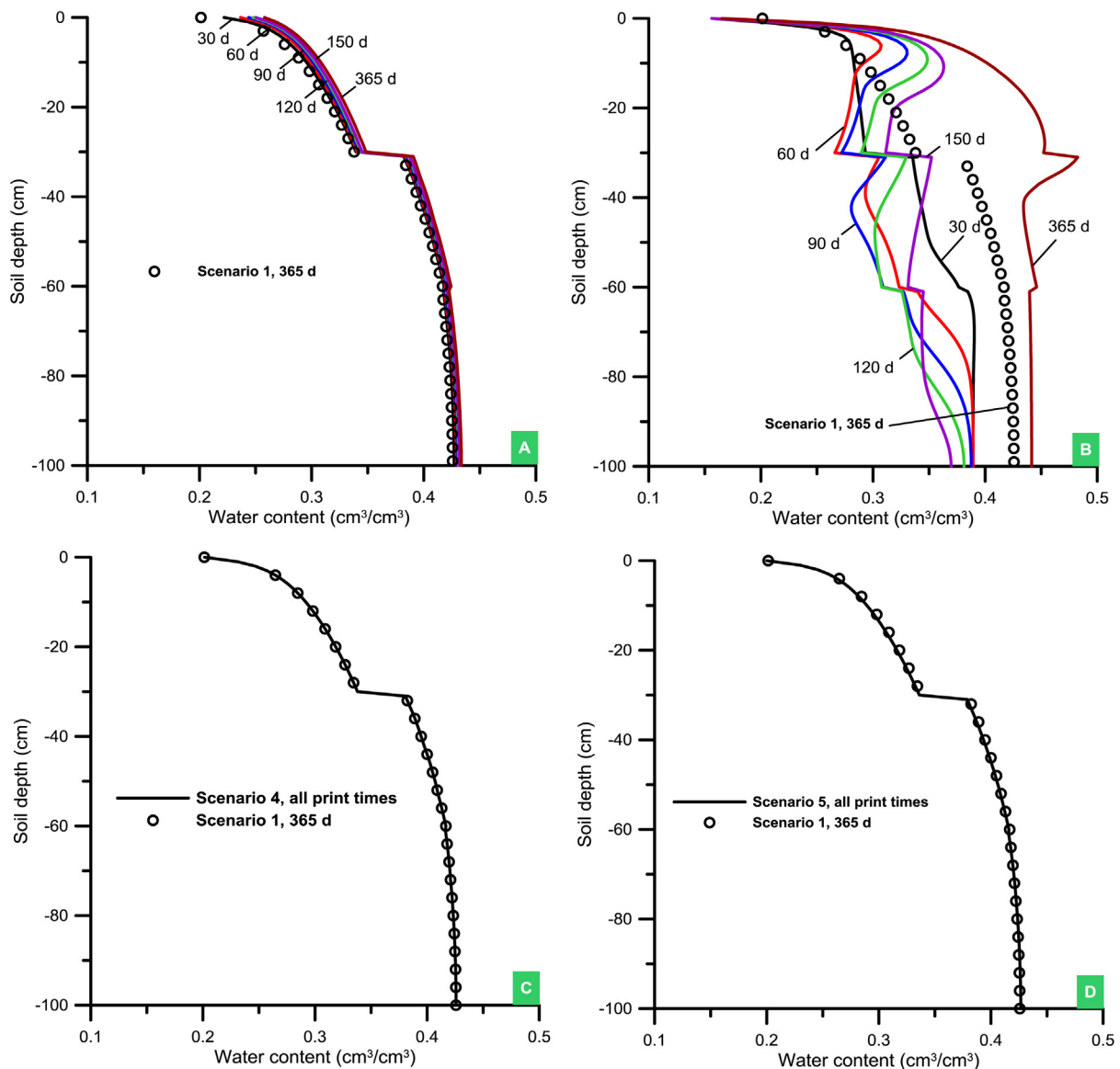
Fig. 4. Water content profiles for Scenarios 2 (A), 3 (B), 4 (C) and 5 (D) and their comparison with the water content profile for Scenario 1 at 365 days.

Water content at a particular depth in the soil profile seems quite constant during the simulation (except for Scenario 3, Fig. 4); however, this is only so because we output water content profiles at the same time of the irrigation cycle (i.e. just before irrigation starts, see Supplementary Material Figure S3). On the other hand, there is a gradual increase in water content with depth as a result of the plant water uptake in the top 0.5 m (rooting depth is from 0 to 0.5 m).

The simulated SAR and EC evolutions illustrate high SAR values of over 100 (Fig. 5A and B) and EC values exceeding 10 dS/m by the end of the simulation period (Fig. 6A and B). The rate at which SAR moves through soil is determined by the migration of Na, Ca, and Mg. Because Na, Ca, and Mg migration is retarded compared to the tracer (Fig. 7A), SAR migration (Fig. 5A) will be retarded too compared to the tracer. The precipitation of Ca in the top of the profile further influences the value of SAR: a decrease in dissolved Ca as a result of calcite production (Fig. 8) increases SAR. Note that pH and bicarbonate concentrations are internally calculated even though inputting such data is not required. The SAR ANZECC trigger value of 20 (sandy-sandy loam soil, see Table 1) is exceeded relatively quickly, i.e. down to a depth of 0.4 m after 150 days.

The electrical conductivity (Fig. 6) progresses much faster than SAR because it is mainly determined by the non-reactive and faster moving chloride; the EC reaches half its maximum concentration (6 dS/m) at the bottom of the profile after 150 days (Fig. 6A), while after 150 days the SAR value is at half its maximum (SAR = 60) between 0.3–0.4 m depth (Fig. 5A). The EC ANZECC trigger value of 0.65 dS/m (see Table 1) is exceeded very quickly after the start of irrigation, i.e. from the surface down to 0.7 m after 30 days.

From the six minerals considered in the Major Ion Chemistry (calcite, dolomite, gypsum, nesquehonite, hydromagnesite, sepeolite), only calcite is formed. The concentration of calcite gradually increases with depth as more irrigation water enters the soil (Fig. 8A). The effect of calcite precipitation is clearly reflected in the concentration of dissolved calcium ions (Fig. 7A): close to the surface, dissolved calcium is nearly absent as a result of precipitation of calcite. Using a calcite mineral density 2.72 g/cm³, total porosity (based on saturated water content) and soil bulk density from Table S2 (Supplementary Material), the calculated mineral volume of precipitated calcite after 365 days was shown to have increased to approximately 0.015 cm³/cm³ at the soil surface. In other words, the mineral phase occupies nearly 3% of total soil
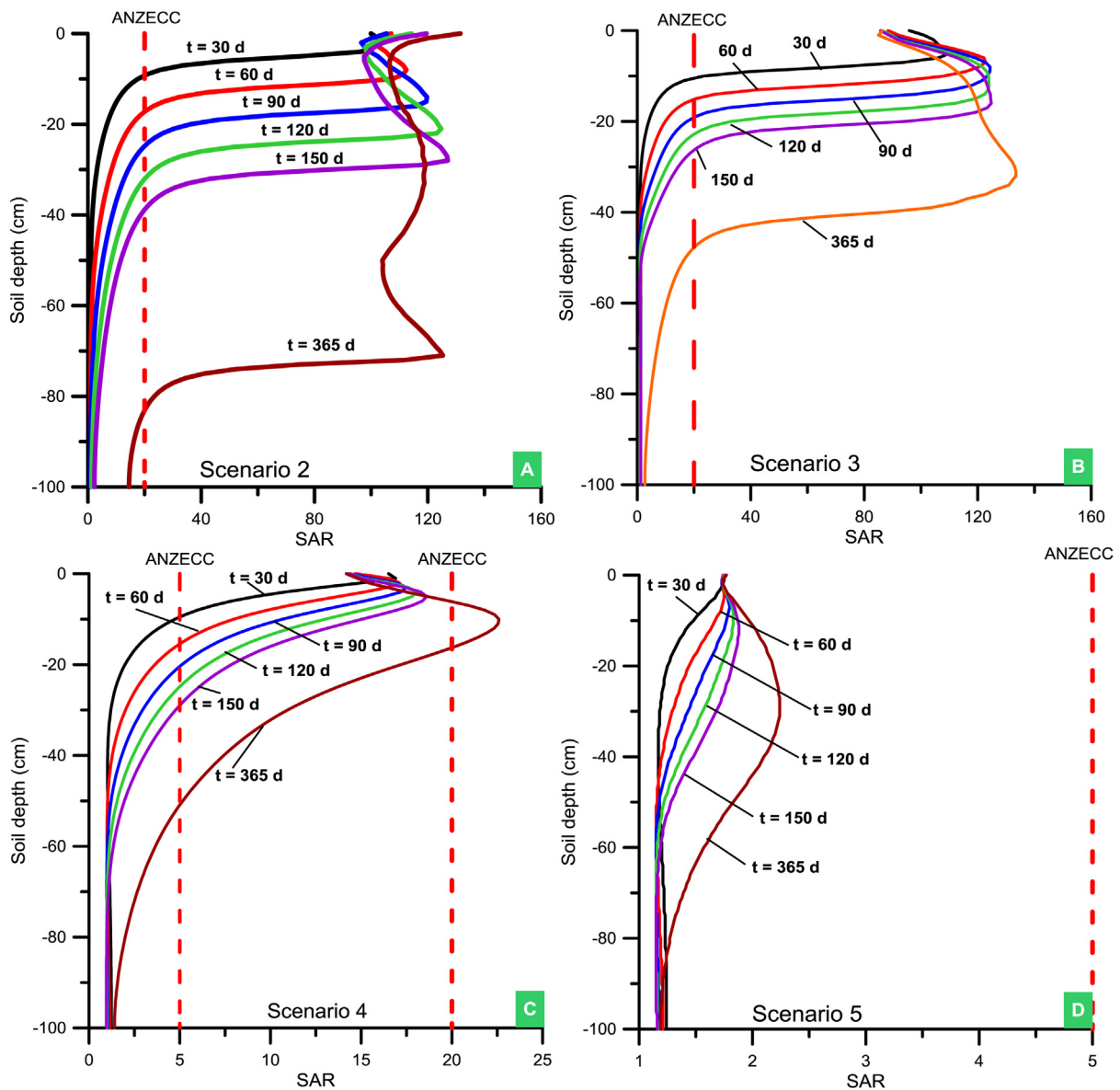
Fig. 5. Simulated SAR for Scenario 2 (A), Scenario 3 (B), Scenario 4 (C) and Scenario 5 (D). ANZECC (2000) guide value for SAR is 5 for light clay and 20 for sand-sandy loam soil. Note different scales in different figures.

porosity (0.515 cm³/cm³ in soil layer 1). While this is a relatively small fraction of the available pore space, this volume is expected to increase if irrigation continues for many years. These long-term effects of salt formation on soil hydrology and plant response need further corroboration.

There are clear differences in the way the major cations Ca, Mg, Na and K migrate through the soil (Fig. 7). Calcium is mainly affected by precipitation in the top soil; ahead of the precipitation front calcium is only weakly retarded compared to chloride. Magnesium displays accumulation at the soil surface due to a decrease in soil water owing to ET; the similarity between magnesium and chloride indicates the former is little retarded. Sodium displays the largest retardation as is expected from the larger Gapon cation exchange constant (see Table 3). The migration of potassium is somewhat similar to Mg, although it exhibits nearly constant values in the top 0.3 m of the soil profile.

3.3. Major ion chemistry effects on soil hydrology

Scenario 3 was run using the Major Ion Chemistry module allowing calculation of concentrations of major ions associated with irrigation of untreated produced water, while now also considering reduction of the hydraulic conductivity due to solution composition (based on the McNeal model, Eq. (3)). During the simulations and based on an irrigation rate of 6 cm/day once in five days, the hydraulic conductivity was reduced automatically due to the salinity effect up to the point that water could not get into the profile without causing ponding. Therefore, we reduced the irrigation rate to 4 cm/day once in five days to avoid ponding conditions. Under these new soil hydrological conditions, the following observations were made regarding the soil water balance and major ion chemistry. Changes in SAR and electrolyte concentration will also affect clay swelling, which in turn may affect the soil water retention curve. Because the focus of this study was on reduction of the
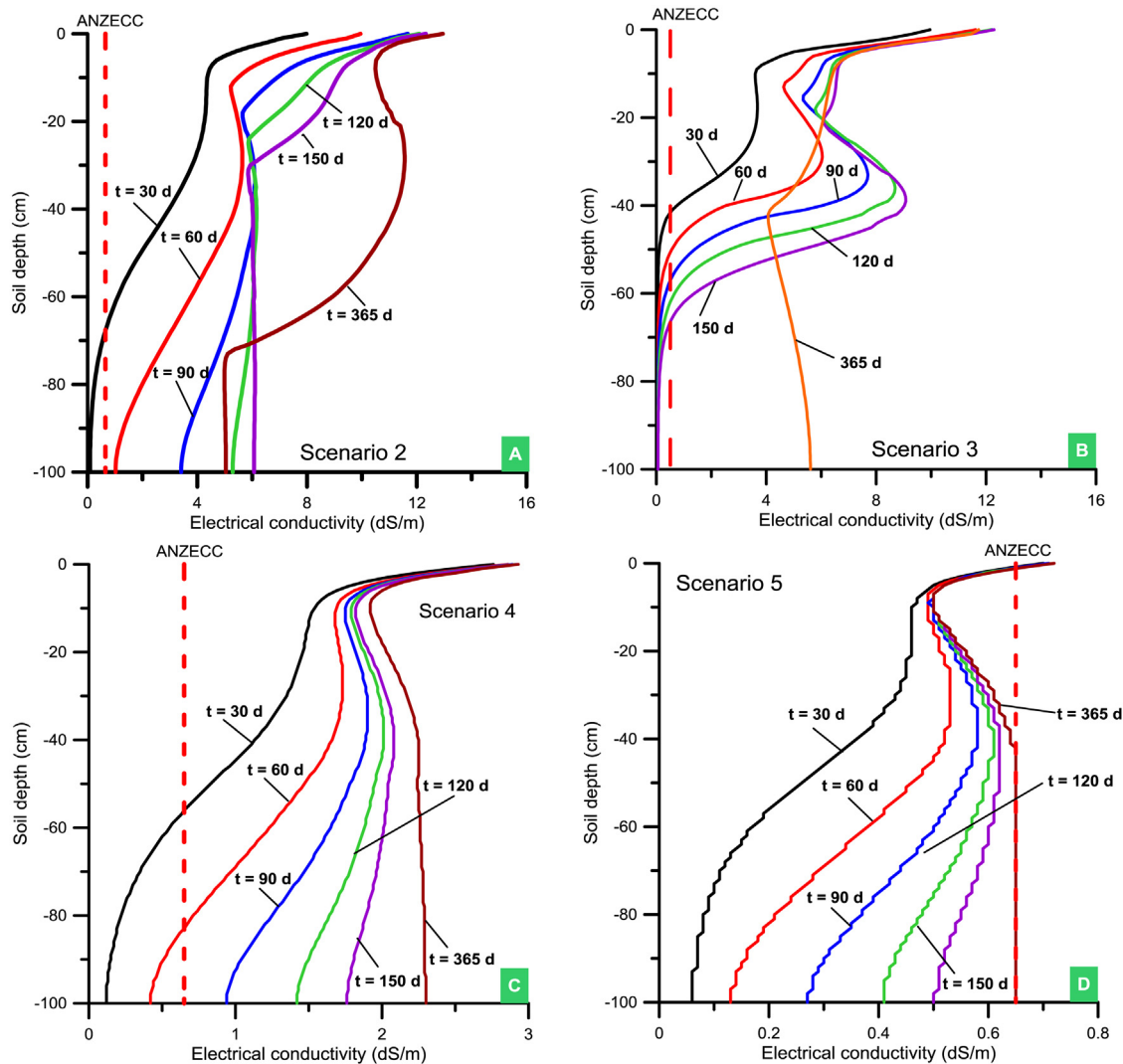
Fig. 6. Simulated electrical conductivity for Scenarios 2 (A), 3 (B), 4 (C) and 5 (D). ANZECC (2000) EC trigger value of 0.65 dS/m. Note different scales in different figures.

hydraulic conductivity, effects on water retention curve were not considered.

The cumulative actual transpiration becomes severely reduced, i.e. down to 188 cm for Scenario 3 compared to 240 cm for Scenario 2 (Fig. 2C and Table 4). The decrease in root water uptake between 0.2 and 0.4 m soil depth (Fig. 9B) is not due to the salinity stress caused by a too high EC. This decrease occurs at the very end of the simulation, when the SAR front reaches the second soil layer, causing the hydraulic conductivity to decrease, which in turn causes water logging in this soil layer. The pressure head associated with this water-logged layer exceeds the −25 cm parameter P1 (Fig. 9A), which caused the water stress response function $\alpha(h)$ to decrease below its optimal rate (i.e. less than one): this, in turn, caused a reduction in plant water uptake rate $S(h)$ (a deviation from its potential value (straight line at $t = 0$ days, with $S(h) = 0.032$ day^{-1} at $z = 0$ in Fig. 9B) and a reduction in actual transpiration.

Compared to the two previous scenarios, the SAR moves downwards about two times slower compared to Scenario 2, while the magnitude is more or less similar (Fig. 5B). The electrical conductivity displays a different distribution across the profile: higher EC values exist at 0.4 m depth while at greater depths EC values are much smaller (Fig. 6B).

3.4. Irrigation with amended produced water

Scenario 4 considers the use of amended irrigation water (based on a 3:1 surface water:produced water ratio) with the chemical composition defined in Table 2, while all other processes and parameters are identical to those of Scenario 3. The cumulative potential and actual surface and bottom fluxes shown in Table 4 reveal that the use of lower salinity irrigation water results in a significantly reduced salinity stress: the actual transpiration is nearly equal to its maximum value (281 cm, as in Scenario 1), 41 cm greater than in Scenario 2 (untreated produced water) and 93 cm greater than in Scenario 3 (untreated produced water with consideration of the hydraulic conductivity reduction model). As a result, the drainage across the bottom of the soil profile is 39 cm lower than in Scenario 2 (for the same amount of irrigation water). Compared to Scenario 2, this scenario results in a more efficient use of the applied irrigation water.

The simulated SAR profiles shown in Fig. 5C demonstrate that the SAR ANZECC trigger value (SAR = 20) for sand-sandy loam is exceeded after 365 days, but only in a small section of the profile. The SAR ANZECC trigger value (SAR = 5) for light clay is exceeded in the top 0.3 m after 150 days, whereas after 365 days it is exceeded in the top 0.5 m.
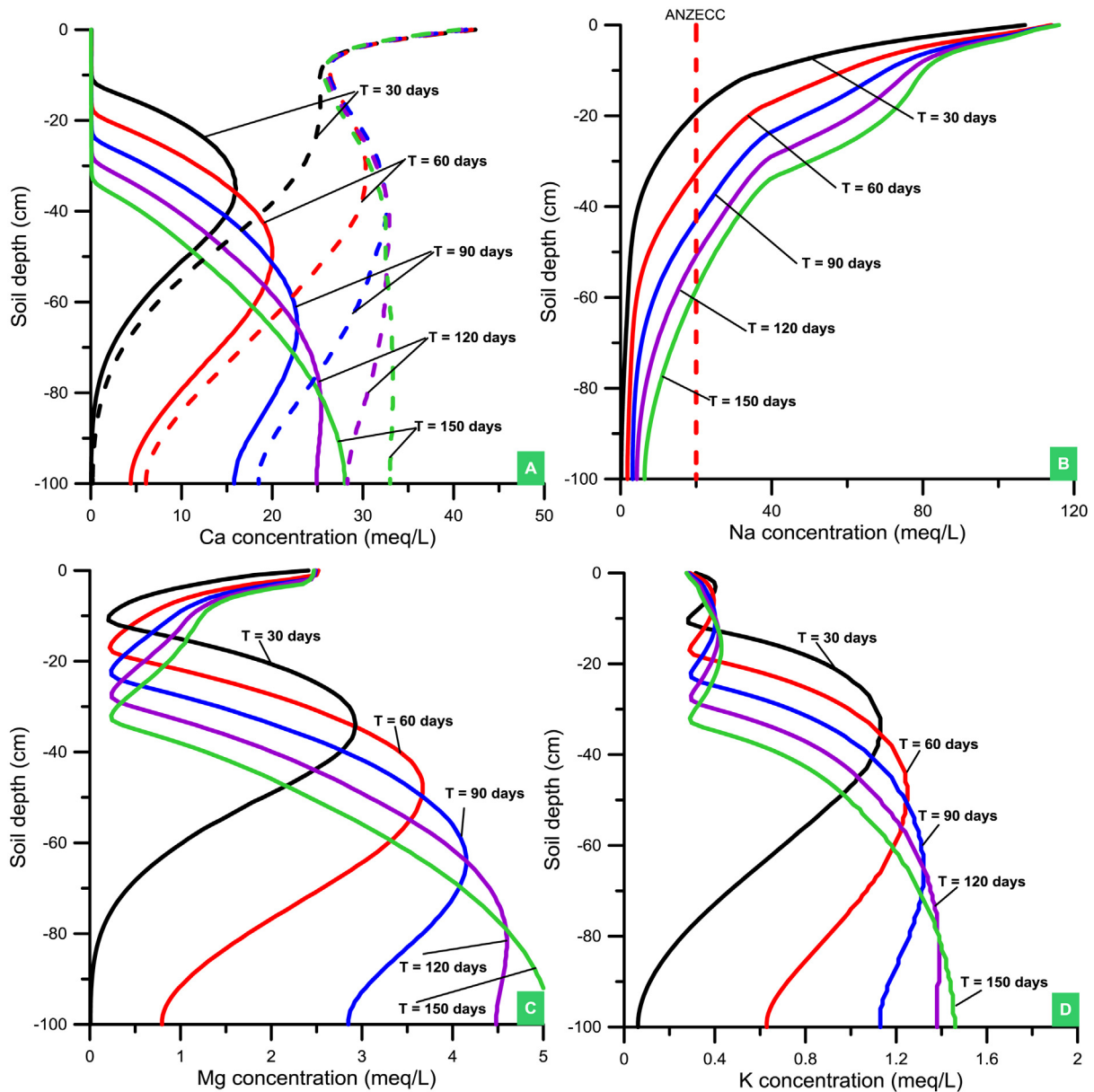
Fig. 7. Simulated concentrations of dissolved major ions Ca (A), Na (B), Mg (C), K (D), and Cl (A, dashed line) for Scenario 2. ANZECC (2000) sodium trigger value of 20 meq/L (B). Dashed lines are for chloride.

The EC ANZECC trigger value of 0.65 dS/m is exceeded across the entire soil profile after 90 days. The relatively high EC is due to the (still relatively high) EC of the irrigation water (1.57 dS/m). In terms of contributions of individual ions in the amended irrigation water to the EC, the most important contributors to EC are sulfate (a 36% contribution to total EC), sodium (a 26% contribution to total EC) and chloride (a 23% contribution to total EC) (Table 2).

Optimisation of irrigation water quality can be done by reducing concentrations of those ions that contribute most to the total EC. In the above example, in decreasing order of importance, that is sulfate, sodium, and chloride, where the contribution of each ion to the total EC is calculated using the procedure given in Table 2.

3.5. Irrigation with treated produced water

In Scenario 5 irrigation water has the chemical composition of water treated by reverse osmosis, as defined in Table 2, while all other processes and parameters are identical to those of Scenarios 3 and 4. The water balance is very similar to Scenario 4, with cumulative actual transpiration equal to 280 cm and drainage flux equal to −84 cm (Fig. 2D and Table 4). Time series of soil water content and pressure head at the 10 cm depth display wetting-drying cycles as a result of the applied irrigation regime and water redistribution due to evapotranspiration and drainage (Fig. 10). Every irrigation event adds solutes to the soil which partly migrate downwards while another part accumulates in the top of the soil profile. The pressure head data indicates that the maximum pressure (about −15 cm) is slightly smaller than the pressure head below which root water uptake is optimal (P1 = −25 cm) (Fig. 10). On the other hand, the minimum pressure head (about −272 cm) exceeds the limiting pressure head below which root water uptake is no longer optimal (P2 = −200 cm). In other words, the water uptake by the grass vegetation considered here occurs at a maximum rate for about 3 out of 4 days, whereas on the 4th day it is suboptimal (see schematic root water uptake function in Supplementary Material Figure S2).
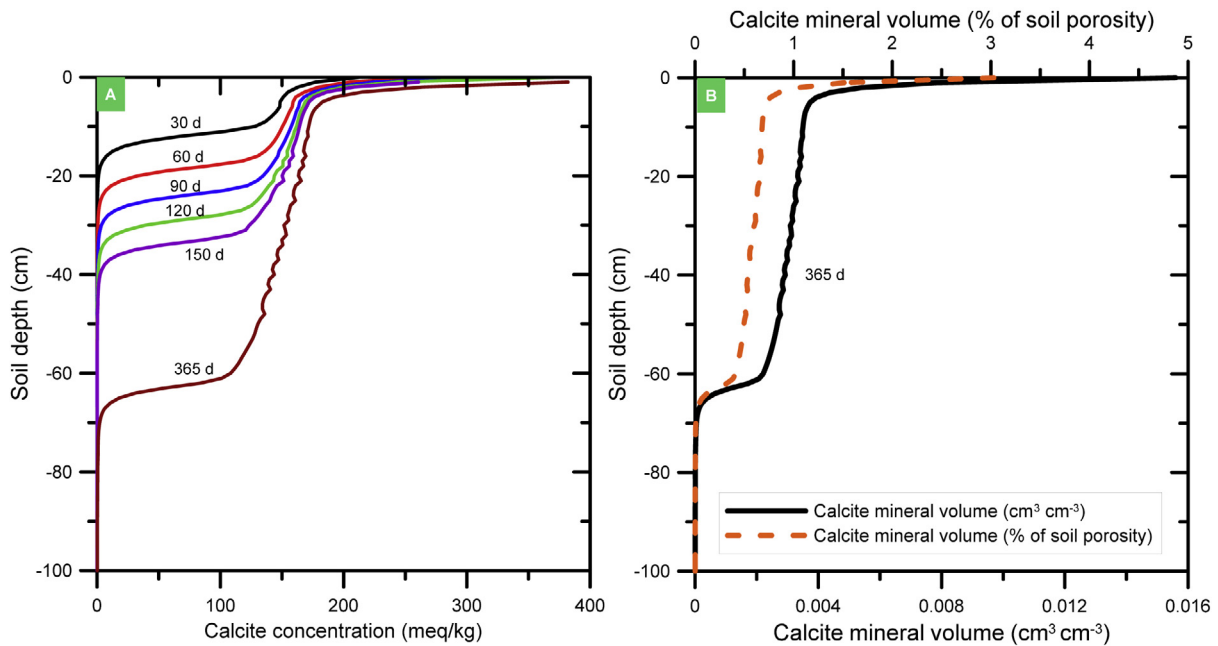
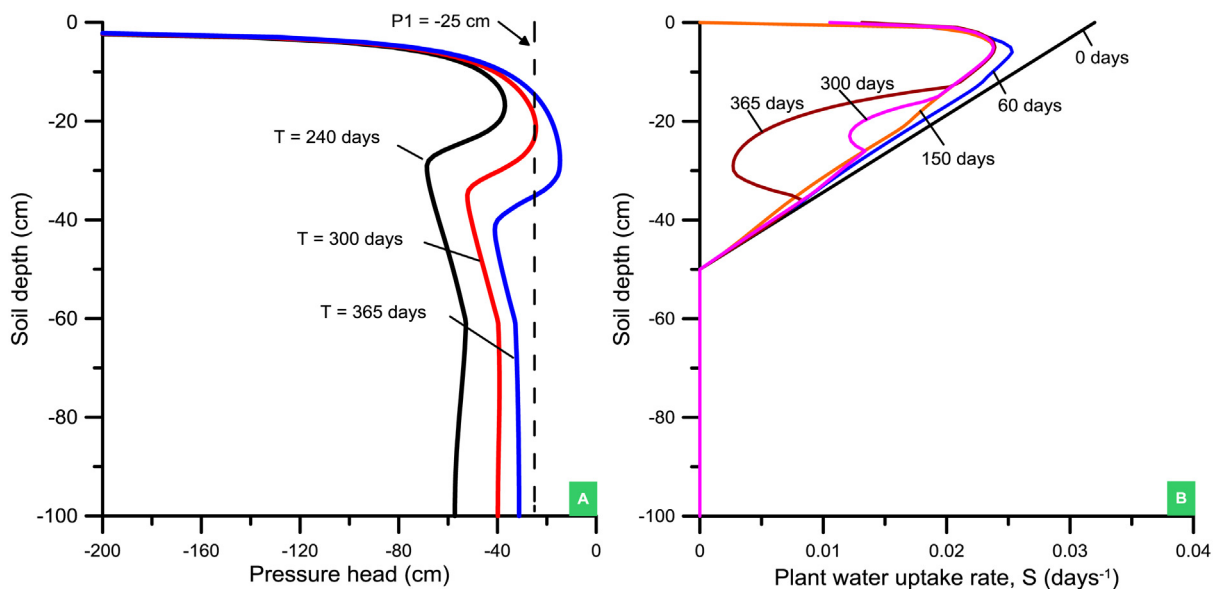Fig. 8. Calcite concentration for Scenario 2 (A). Calcite mineral volume after 365 days of irrigation (B).

Fig. 9. Pressure head (A) and root water uptake (B) profiles for Scenario 3. The pressure head exceeds the P1 = −25 cm threshold after 300 days (A).

A more optimal irrigation regime would involve starting irrigation at day 4 to avoid the soil from becoming too dry.

The simulated SAR profiles now remain below the lowest SAR ANZECC trigger value (SAR = 5) for light clay (Fig. 5D). This result is as expected, given the low SAR value (i.e. 1.6) of the irrigation water and the absence of any initial salt build-up in the soil profile (the initial SAR value is 1.25 throughout the entire soil profile) or without other salt inputs into the soil profile (e.g. from saline shallow groundwater or lateral inflow from water discharging at the break-of-slope, Biggs et al., 2012).

The EC ANZECC trigger value of 0.65 dS/m is generally not exceeded across the entire soil profile, except at the very top few centimetres. Although the EC of the irrigation water is low (0.29 dS/m), EC in the top of the soil profile increases to a maximum value of 0.73 dS/m due to evapotranspiration leading to dry

soil conditions, triggering salts to concentrate near the soil surface. In terms of contributions of individual ions in the treated irrigation water to the EC, the most important contributors to EC are chloride (a 49.6% contribution to total EC), sodium (a 21.5% contribution to total EC) and magnesium (a 11.3% contribution to total EC) (Table 2).

Depth distributions of aqueous concentrations of major cations Ca, Mg, Na and K in the soil profile are shown in Fig. 11. Calcium, magnesium, and sodium display similar patterns; an accumulation at the soil surface due to a decrease in soil water owing to ET and gradual accumulation at deeper depths due to downward leaching. Sodium displays the largest retardation as is expected from the Gapon cation exchange constant (see Table 3). The migration of potassium is somewhat different in the top 0.3 m of the soil profile, without a distinctive accumulation as observed with the other
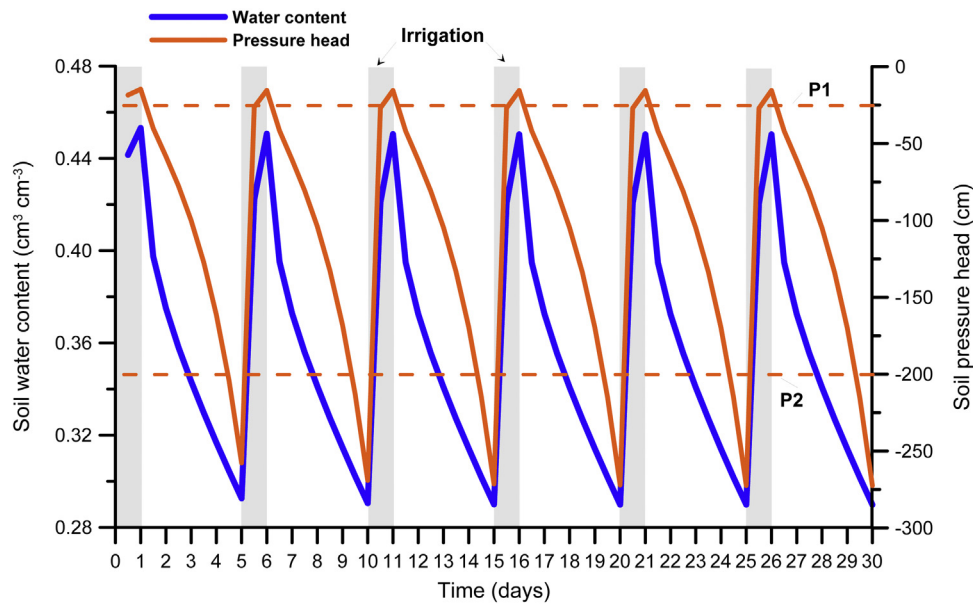
Fig. 10. Calculated soil water contents and pressure heads at the 10 cm depth (Scenario 5; pasture). Every five days a 24-h irrigation event takes place. P1 = pressure head below which root water uptake is optimal and P2 = limiting pressure head below which root water uptake is no longer optimal.

ions. The sodium ANZECC trigger value of 20 meq/L (460 mg/L, see Table 1) is not exceeded anywhere in the soil profile.

Fig. 12 shows concentrations of sorbed/exchangeable cations on the cation exchange sites. While the concentration front for exchangeable Na moves relatively quickly down the soil profile, the front reaching half the total soil depth after 365 days, other concentration fronts (i.e., for Ca and Mg) move much slower. This is mainly due to large amounts of Na being added with irrigation water and relatively small buffering capacity with respect to Na (note that the initial concentration for exchangeable Na was only about 2.6 meq/kg). On the other hand, the initial concentrations of exchangeable Ca and Mg were about 175 and 89 meq/kg, resulting in a significantly larger buffering capacity for these two cations compared to Na.

From the six minerals considered in the Major Ion Chemistry (calcite, dolomite, gypsum, nesquehonite, hydromagnesite, sepeolite), only calcite is formed in Scenario 5. However, the concentration of calcite is very small as it reaches only 0.5 meq/kg (results not shown), compared to several hundred meq/kg for Scenario 2.

3.6. Summary of water and chemical mass balance calculations

For each scenario, water balance components were calculated based on a 365-day simulation period. Cumulative infiltration, actual transpiration (root water uptake), evaporation and net drainage (outflow–inflow) values are shown for each of five scenarios evaluated (Table 4). The cumulative actual transpiration and evaporation are each also expressed as a percentage of their respective cumulative potential values (292 and 73 cm, respectively).

For all scenarios except Scenario 3 cumulative infiltration equals the imposed value of 438 cm based on a 6 cm/day irrigation rate once every 5 days. Scenario 3 had a reduced irrigation rate of 4 cm/day once every 5 days resulting in a lower cumulative infiltration of 292 cm. The lower irrigation rate was required to avoid ponding conditions as a result of the reduction in hydraulic conductivity when untreated produced water was applied.

The cumulative actual transpiration is a useful metric to evaluate combined effects of soil chemical and soil physical processes on the soil water balance and on plant water stress. In all scenarios

the cumulative actual transpiration is less than its potential value; for Scenarios 1, 4, and 5 transpiration reaches 281 cm or 96% of the potential value. The observation that the plant experiences a very small water stress is most likely due to the sub-optimal irrigation regime which generates soil pressure heads slightly outside the optimal range, especially near the more negative soil pressure heads where the limiting pressure head P2 becomes exceeded (see Fig. 10). Larger differences between actual and potential transpiration exist for Scenario 2 (82% of potential value) and 3 (64% of potential value). Scenario 2 applied the combined water and solute stress model - in combination with the major ion chemistry module - to control root water uptake: this resulted in an additional stress on plant water uptake, mainly caused by a salinity stress (irrigation water EC = 5700 μS/cm). Smaller actual transpiration for Scenario 3 (188 cm) is due in part to (i) the increased water stress as a result of a drier soil (4 cm/day rather than 6 cm/day irrigation rate, every 5 days), (ii) sup-optimal pressure head conditions owing to a decrease in the hydraulic conductivity, generating near-saturated conditions within the root zone, and (iii) to a salinity stress (irrigation water EC = 5700 μS/cm).

Cumulative actual evaporation reached its maximum value of 73 cm (based on a 0.2 cm/day potential evaporation rate) in all but one scenario (i.e., Scenario 3 yielded 69 cm or 95% of the potential value owing to the reduced infiltration, generating drier soil moisture conditions and hence reduced evaporation).

Cumulative net drainage (the difference between cumulative outflow and inflow) is identical (and negative, defined here as outflow through the bottom of the soil profile) for Scenarios 1, 4, and 5. Higher drainage for Scenario 2 (−123 cm) is due to the lower transpiration, leaving more water in the soil profile that is available for gravity drainage. Much lower drainage for Scenario 3 (−29 cm) is the result of the smaller irrigation rate. Note that the decrease in irrigation by ~33% results in a decreased in drainage of ~65%. Calculated net drainage values from Table 4 are considerably higher than calculated values for furrow irrigation on cracking clay soils (e.g., 10–20 cm/year) as reported by (Biggs et al., 2012). Our higher drainage values are the result of the higher irrigation rate applied constantly for a full year.

A comparison of Scenarios 1 and 2 is interesting from another perspective: it illustrates the effect of including or excluding certain
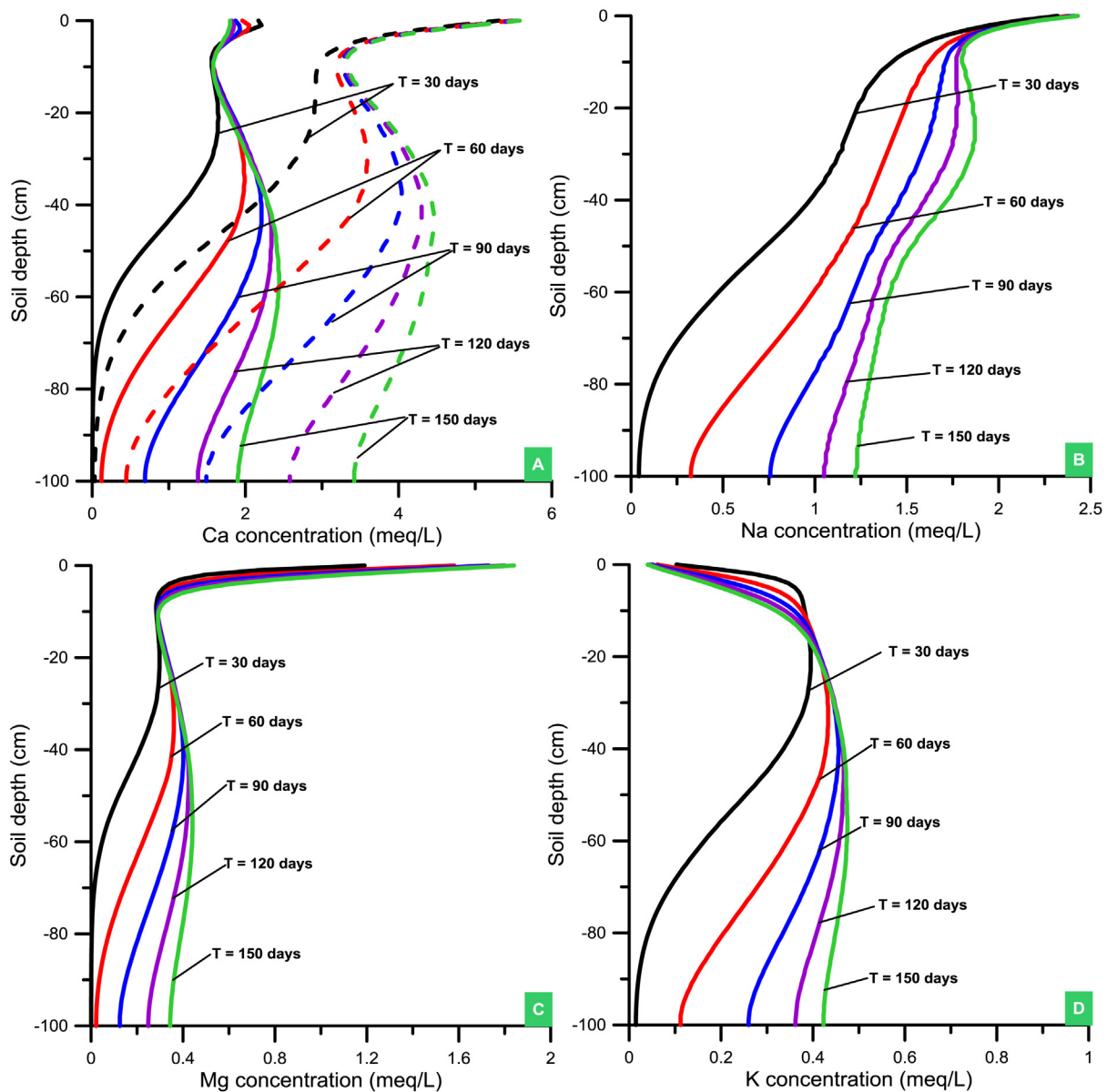
Fig. 11. Simulated concentrations of dissolved major ions Ca (A), Na (B), Mg (C), K (D), and Cl (A), Scenario 5. Dashed lines are for chloride.

coupled soil processes on soil water balance components. Scenario 1 has a standard advection–dispersion solute transport model without major ion chemistry; the irrigation water is solute-free and only contains a tracer. Scenario 2, on the other hand, accounts not only for major ion chemistry but also calculates salinity effects on root water uptake. Scenario 2 is an example where a link is made between soil geochemistry, soil hydrology, and plant water uptake. Accounting for such coupled processes resulted in (i) a decrease of the actual transpiration to 82% of its potential value, and (ii) an increase in net drainage by 46% compared to Scenario 1. This is a clear demonstration that soil water balance modelling involving major ion chemistry should account for the above interacting processes. Note that the importance of such interacting processes decreases as the applied irrigation water has a less extreme chemical composition (such as the amended and treated produced water).

Mass fluxes of major cations and anions were calculated for upper and lower model boundary (Table 5). This is important for estimating the potential effects of salt leaching from upper soil layers to deeper soil layers as leaching may negatively affect the concentration of adsorbed sodium and the soil hydraulic conduc-

tivity of deeper soil layers. To better protect groundwater resources from pollution with salts and nutrients, it is further important to estimate the potential mass flux of salts leaching to shallow groundwater. For all scenarios, the mass flux for calcium out of the soil is larger than the mass of calcium added via irrigation. This results from calcium being replaced on the adsorption complex by mono-charged sodium cations whose added mass via the irrigation water is two orders of magnitude larger than that of calcium. As the sodium concentration in the irrigation water decreases when untreated produced water is replaced by surface-water amended produced water (Scenario 4) or treated produced water (Scenario 5), the calcium mass flux through the bottom of the soil profile decreases due to decreased competition for adsorption sites between calcium and sodium. For magnesium, the mass flux through the bottom of the soil profile is larger than that added via irrigation only when untreated produced water is used (Scenarios 2 and 3). Similarly as for Ca, Mg is displaced from the solid phase by the large concentrations of Na. For all other scenarios, magnesium accumulates in the soil (input flux is larger than output flux via drainage). As a result of the displacement of Ca and Mg
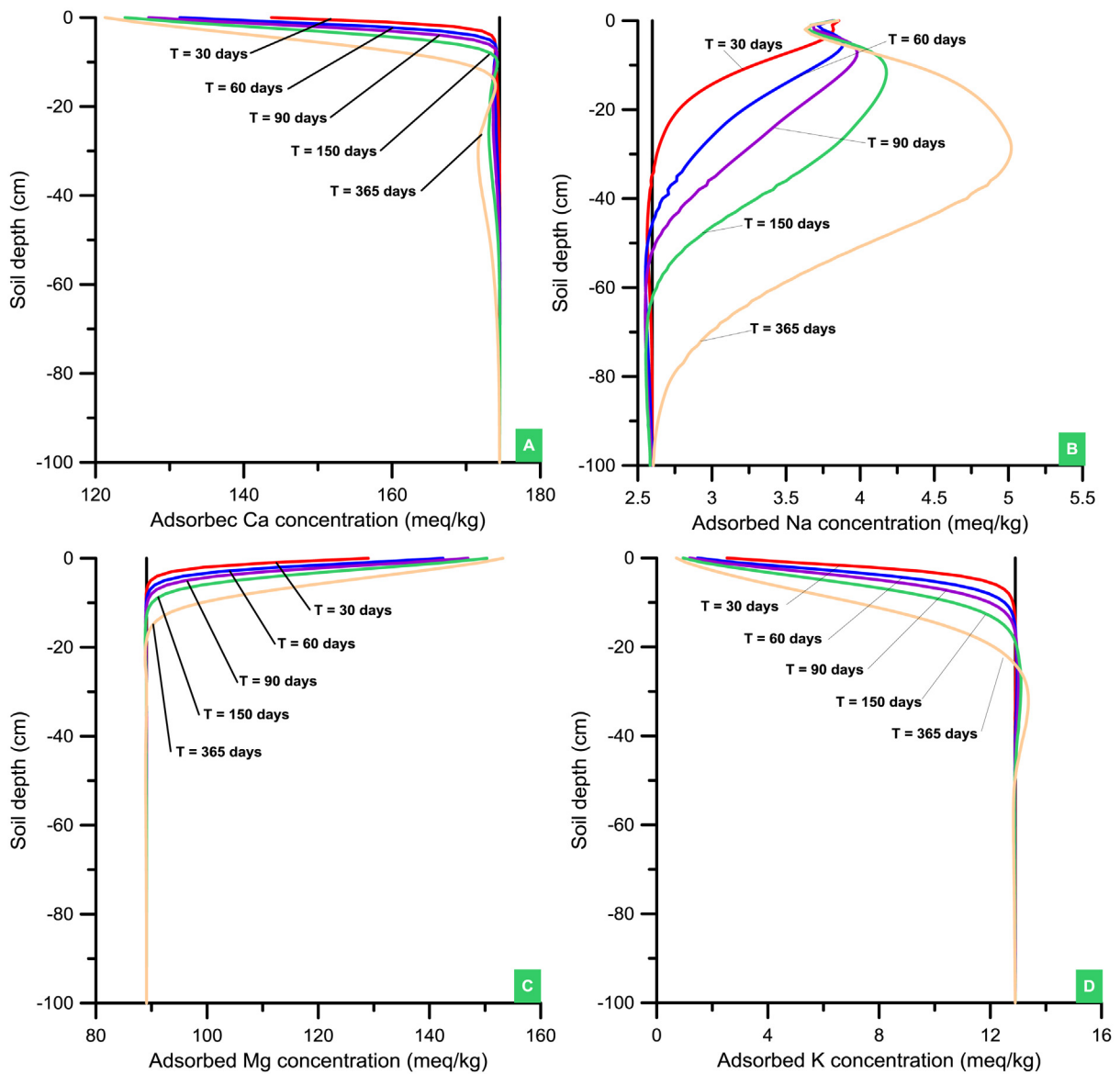
Fig. 12. Surface species concentrations for Ca (A), Na (B), Mg (C) and K (D) versus soil depth during irrigation cycles. The total adsorbed concentration for Ca + Na + Mg + K is constant (275 meq/kg for soil layer 1, 278 meq/kg for soil layer 2, and 274 meq/kg for soil layer 3) (Scenario 5).

Table 5

Chemical mass fluxes (g/m^2) through upper and lower model boundary for a 365 day simulation period. Negative fluxes for the upper model boundary are inputs to the soil; negative values for the lower model boundary refer to fluxes leaving the soil. For each element and each scenario, the first row is a flux through the upper boundary (input); the second row is a flux through the lower boundary (output).

Scenario	Ca	Mg	Na	K	HCO$_3$	SO$_4$	Cl
2: Pasture – UPW–MIC–WSS	−4.56E+01	−3.93E+01	−6.18E+03	−2.41E+01	−5.64E+03	−9.99E+01	−2.61E+03
	−6.76E+02	−7.91E+01	−6.90E+02	−7.35E+01	−1.44E+01	−7.92E+01	−2.07E+03
3: Pasture – UPW–MIC–WSS–KRM	−3.02E+01	−2.59E+01	−4.07E+03	−1.59E+01	−3.72E+03	−6.58E+01	−1.72E+03
	−4.42E+02	−4.99E+01	−1.69E+02	−3.19E+01	−2.92E+00	−3.80E+01	−9.93E+02
4: Pasture – SAPW–MIC–WSS–KRM	−4.52E+01	−2.86E+01	−8.09E+02	−1.53E+02	−6.04E+02	−1.48E+03	−7.20E+02
	−2.06E+02	−2.07E+01	−5.52E+01	−2.55E+01	−1.01E+01	−9.13E+02	−4.43E+02
5: Pasture – TPW–MIC–WSS–KRM	−4.54E+01	−3.33E+01	−1.26E+02	−1.90E+00	−8.24E+01	−4.39E+00	−2.95E+02
	−5.70E+01	−6.27E+00	−2.80E+01	−1.63E+01	−1.17E+01	−2.74E+00	−1.75E+02

UPW: untreated produced water; MIC: major ion chemistry; WSS: water and solute stress model; KRM: hydraulic conductivity reduction model; SAPW: surface water amended produced water; TPW: treated produced water.

by Na, sodium accumulates on the exchanger resulting in a tenfold smaller sodium flux at the bottom of the soil profile compared to its input flux (Scenario 2). The behaviour of potassium is similar to that of magnesium: as a smaller mass of potassium goes into the soil under Scenarios 4 and 5, the mass flux of potassium leaving the soil profile decreases. When comparing the effect of using different water types on salt leaching, the use of treated produced water clearly generates the overall smallest mass fluxes (for all ions except HCO_3) from soil to groundwater. This is not just the result of a smaller input of solutes via the treated produced water, but also because decreased sodium concentrations displace smaller amounts of major ions previously present on the soil's exchange complex.

4. Conclusions

An in-depth analysis has been undertaken to provide information for potential optimisation of irrigation water quality that will yield minimal long-term effects of dissolved ions on soil and plant health. Three different irrigation water qualities were evaluated, where the water source was considered to be produced coal seam gas water: untreated or treated produced water or produced water amended with surface water. The analysis also involved the use of two different conceptualisation of water quality evolution in the soil. The first conceptualisation served as a baseline and did only consider the coupled variably-saturated water flow and standard advection–dispersion transport models implemented in HYDRUS-1D. The second conceptualisation considered the HYDRUS-1D code and its major ion chemistry module UnsatChem to simulate the simultaneous movement of multiple major ions (Na, K, Ca, Mg, Cl, SO_4, alkalinity) present in irrigation water in a vegetated soil profile (pasture).

Simulations with different irrigation water qualities provided detailed results regarding chemical indicators of soil and plant health, i.e. SAR, EC and sodium concentrations. By comparing such indicators in the soil profile with water quality guideline values (here the Australian and New Zealand ANZECC values), an assessment was made of the suitability of the applied produced water for long-term irrigation. The assessment evaluated the build-up of salts in the soil profile and its effect on the plant salinity stress, a condition which reduces the capacity of plants to uptake water and results in yield reduction. Finally, the simulations also allowed to test under which conditions soil hydraulic properties, in particular, the hydraulic conductivity, are negatively impacted by salt concentrations owing to clay dispersion. Changes in the soil water retention characteristics were not modelled.

One of the three irrigation scenarios considered the use of untreated produced water (EC = 5705 μS/cm and SAR = 77). Because irrigation with produced water is strictly regulated, the purpose of this scenario was to provide useful insights into the type of coupled chemical-hydrological processes that might occur, and what the potential impacts would be on soil and plant health should such water end up in the soil. For example, by using saline irrigation water, we demonstrated that accumulation of monovalent ions causes clay swelling, resulting in a decrease in hydraulic conductivity of a particular soil layer. This, in turn, caused water stagnation above this layer (the pressure head exceeds the threshold for optimum water uptake by plant roots), leading to an additional plant water stress and reduced transpiration (188 cm versus 240 cm without the water stress, or more than 20% less). Due to lower transpiration, more water resides in the soil profile after irrigation, causing drainage to increase by 46% (-123 cm compared to -84 cm).

In case when produced water was amended with surface water (at a ratio of 3:1 of surface water:produced water, with EC = 1573 μS/cm and SAR = 11), the calculated soil SAR values were much lower and generally acceptable for sandy to sandy-loam soil (i.e. less than 20). Permissible SAR values for light clay (i.e. less than 5) were still exceeded in most of the soil profile. Results also demonstrated the formation of calcite in the top of the soil profile owing to solute concentration effects under dry soil moisture conditions. This case did not result in an additional stress on plant water uptake as a result of the acceptable salinity levels.

A final case used treated produced water with a relatively low concentration of major ions (EC = 291 μS/cm, SAR = 1.6). The permissible SAR values for light clay were not exceeded, and all other ions remained at tolerable levels. Under these conditions, actual transpiration was not reduced by an additional salinity stress, meaning that near optimal soil hydrological and chemical conditions existed for plant growth.

Our analysis further illustrates that accounting for coupled geochemical, hydrological and plant water uptake processes resulted in (i) a decrease of the actual transpiration to 82% of its potential value, and (ii) an increase in net drainage by 46% when compared to a water balance calculation where such interacting processes were disregarded. This is a clear demonstration that soil water balance modelling involving major ion chemistry should account for the above interacting processes.

The major ion chemistry module UnsatChem implemented in HYDRUS-1D is a very powerful tool to assess in a very detailed way potential effects of different irrigation water qualities on soil and plant health. This offers a cost-effective way to optimise the quality of irrigation water derived from coal seam gas water or other saline waters and thus to ensure soils are managed in a sustainable manner. To further underpin such assessments, field trials providing detailed soil chemical and physical data need to be considered to test the validity of the simulations and to improve process parameterisation. One of the processes that needs improvement and testing is the change in hydraulic properties as a result of mineral precipitation/dissolution causing partial or full pore blockage. Based on a simulation period of a single year, calcite precipitation was found to occupy up to 3% of the soil's pore space in the top of the soil profile. The long-term evolution of salinity and its effect on soil hydraulic properties also needs further corroboration.

Acknowledgements

Appendix A. Supplementary data

Supplementary data associated with this article can be found, in the online version, at http://dx.doi.org/10.1016/j.agwat.2017.04.011.

References

Appelo, T., Postma, D., 2004. Geochemistry, Groundwater, and Pollution, second ed.

ANZECC, 2000. Australian and New Zealand Guidelines for Fresh and Marine Water Quality. Volume 1: The Guidelines (Chapters 1–7).

Beletse, Y.G., Annandale, J.G., Steyn, J.M., Hll, I., Aken, M.E., 2008. Can crops be irrigated with sodium bicarbonate rich CBM deep aquifer water? Theoretical and field evaluation. Ecol. Eng. 33, 26–36.

Bennett, S., (Ph.D. thesis) 2012. Key Spatiotemporal Factors Determining Uncertainty of Deep Drainage in a Semi-arid Area. The University of New South Wales.

Biggs, A., Witheyman, S.L., Williams, K.M., Cupples, N., de Voil, C.A., Power, R.E., Stone, B.J., August 2012. Assessing the Salinity Impacts of Coal Seam Gas Water

on Landscapes and Surface Streams. Final Report of Activity 3 of the Healthy HeadWaters Coal Seam Gas Water Feasibility Study. Department of Natural Resources and Mines, Toowoomba.

BOM, 2014. Bureau of Meteorology, Recent Evapotranspiration, http://www.bom.gov.au/watl/eto/.

Bright, D.A., Addison, J., 2002a. Derivation of Matrix Standards for Salt Under the British Columbia Contaminated Sites Regulation. Royal Roads University.

Bright, D.A., Addison, J., 2002b. Derivation of Matrix Standards for Salt Under the British Columbia Contaminated Sites Regulation. Addendum A: Technical Options Analysis for a Soil Chloride Standard for Drinking Water Protection (Aesthetic). Applied Research Division, Royal Roads University, Victoria, BC.

Burkhardt, A., Gawde, A., Cantrell, C.L., Baxter, H.L., Joyce, B.L., Stewart Jr., C.L., Zheljazkov, V.D., 2015. Effects of produced water on soil characteristics, plant biomass, and secondary metabolites. J. Environ. Qual. 44, 1938–1947, http://dx.doi.org/10.2134/jeq2015.06.0299.

Crosbie, R., Morrow, D., Cresswell, R., Leaney, F., Lamontagne, S., Lefournour, M., 2012. New Insights to the Chemical and Isotopic Composition of Rainfall Across Australia. Water for a Healthy Country Flagship Report Series ISSN: 1835-095X. CSIRO.

DERM, 2010. Guideline: Approval of Coal Seam Gas Water for Beneficial Use. Department of Environment and Resource Management, Queensland, Australia.

DEHP, 2014. General Beneficial Use Approval—Irrigation of Associated Water (Including Coal Seam Gas Water). Department of Environment and Heritage Protection, Queensland, Australia.

DNRM, 2012. Forecasting Coal Seam Gas Water Production in Queensland's Surat and Southern Bowen Basins. Report Prepared by Klohn Crippen Berger: Healthy HeadWaters Coal Seam Gas Water Feasibility Study. Department of Environment and Resource Management, Queensland, Australia.

DNRM, 2013. Assessment of Alternative Use Options for Coal Seam Gas Water Proposed for Central Condamine Alluvium Recharge Schemes. Healthy HeadWaters Coal Seam Gas Water Feasibility Study. Department of Environment and Resource Management, Queensland, Australia.

Feddes, R.A., Kowalik, P.J., Zaradny, H., 1978. Simulation of Field Water Use and Crop Yield. John Wiley & Sons, New York, NY.

Horizon, 2006. Irrigated Pasture Systems Comparative Project. Stage 3 Final Report.

Jacques, D., Smith, C., Šimůnek, J., Smiles, D., 2012. Inverse optimization of hydraulic, solute transport, and cation exchange parameters using HP1 and UCODE to simulate cation exchange. J. Contam. Hydrol. 142–143, 109–125.

Jacques, D., Šimůnek, J., Mallants, D., van Genuchten, M.Th., 2013a. The HPx reactive transport models: summary of recent developments and applications. In: 4th International Conference "Hydrus Software Applications to Subsurface Flow and Contaminant Transport Problems". Czech University, pp. 7–16.

Jacques, D., Perko, J., Seetharam, S., Mallants, D., Govaerts, D., 2013b. Modelling long-term evolution of cementitious materials used in waste disposal. In: IAEA-TECDOC-1701 Behaviours of Cementitious Materials in Long Term Storage and Disposal., pp. 26.

Johnston, C.R., Vance, G.F., Ganjegunte, G.K., 2008. Irrigation with coalbed natural gas co-produced water. Agric. Water Manag. 95, 1243–1252.

Lenhard, R.J., Brooks, R.H., 1986. Effects of clay–solution interactions on water retention. Am. Soc. Civil Eng. J. Irrig. Drain. Eng. 112, 28–38.

Leskiw, L.A., Sedor, R.B., Welsh, C.M., Zeleke, T.B., 2012. Soil and vegetation recovery after a well blowout and salt water release in northeastern British Columbia. Can. J. Soil Sci. 92, 179–190.

Maas, E.V., 1990. Crop salt tolerance. In: Tanji, K.K. (Ed.), Agricultural Salinity Assessment and Management. ASCE Manuals and Reports on Engineering Practice, No. 71. , New York.

Mace, J.E., Amrhein, C., 2001. Leaching and reclamation of a soil irrigated with moderate SAR waters. Soil Sci. Soc. Am. J. 65, 199–204.

McNeal, B.L., 1968. Prediction of the effect of mixed-salt solutions on soil hydraulic conductivity. Soil Sci. Soc. Am. Proc. 32, 190–193.

McNeal, B.L., 1974. Soil salts and their effects on water movement. In: van Schilfgaarde, J. (Ed.), Drainage for Agriculture, Agronomy No. 17. Am. Soc. Agr., Madison, WI.

Minasny, B., McBratney, A., 2002. The neuro-m method for fitting neural network parametric pedotransfer functions. Soil Sci. Soc. Am. J. 66, 352–361.

Moore, T.A., 2012. Coalbed methane: a review. Int. J. Coal Geol. 101, 36–81.

Mualem, Y., 1976. A new model for predicting the hydraulic conductivity of unsaturated porous media. Water Resourc. Res. 12, 513–522.

Nghiem, L.D., Ren, T., Aziz, N., Porter, I., Regmi, G., 2011. Treatment of coal seam gas co-produced water for beneficial use in Australia: a review of best practices. Desalin. Water Treat. 32, 316–323.

Parsons, W., 2010. Chapter 12 in Australia Pacific LNG Project Environmental Impact Statement. Adaptive Associated Water Management, vol. 2. Report to Origin and Conoco Phillips (Asia Pacific LNG Joint Venture), Brisbane.

QWC, July 2012. Underground Water Impact Report for the Surat Cumulative Management Area. Queensland Water Commission.

Ringrose-Voase, A.J., 2004. Water Balance and Deep Drainage Under Irrigated Cotton. 'WaterPak'. In: Dugdale, H., Harris, G., Neilsen, J., Richards, D., Roth, G., Williams, D. (Eds.). Cotton Research and Development Corporation, Narrabri, New South Wales, pp. 17–28.

RPS, 2011. Onshore co-produced water: extent and management. In: LTD, R.A.P. (Ed.), Waterlines Report Series No. 54. National Water Commission, Canberra.

Santos, 2009. Sustainability Report 2009: The Energy for Sustainability, Australia.

Santos, 2010. Upstream-Fairview Project Area Environmental Management Plan; Appendix B Fairview Project Area Coal Seam Gas Water Management Plan.

Silburn, D.M., Montgomery, J., 2004. Deep drainage under irrigated cotton in Australia: a review. In: WATER-PAK a Guide for Irrigation Management in Cotton. Cotton Research and Development Corporation and Australian Cotton Cooperative Research Centre, Narrabri, pp. 29–40.

Šimůnek, J., Suarez, D.L., 1994. Two-dimensional transport model for variably saturated porous media with major ion chemistry. Water Resour. Res. 30, 1115–1133.

Šimůnek, J., Suarez, D.L., 1997. Sodic soil reclamation using multicomponent transport modelling. ASCE J. Irrig. Drain. Eng. 123, 367–376.

Šimůnek, J., van Genuchten, M.Th., Šejna, M., 2008. Development and applications of the HYDRUS and STANMOD software packages and related codes. Vadose Zone J. (Special Issue "Vadose Zone Modeling") 7, 587–600, http://dx.doi.org/10.2136/VZJ2007.0077.

Šimůnek, J., Šejna, M., Saito, H., Sakai, M., van Genuchten, M.Th., 2013. The HYDRUS-1D Software Package for Simulating the Movement of Water, Heat, and Multiple Solutes in Variably Saturated Media, Version 4.17, HYDRUS Software Series 3. Department of Environmental Sciences, University of California Riverside, Riverside, CA, USA, pp. 343.

Šimůnek, J., Jacques, D., van Genuchten, M.T., Mallants, D., 2006. Multicomponent geochemical transport modelling using Hydrus-1D and HP1. J. Am. Water Resour. Assoc. 42, 1537–1547.

Šimůnek, J., van Genuchten, M.Th., Šejna, M., 2016. Recent developments and applications of the HYDRUS computer software packages. Vadose Zone J. 15 (7), 25, http://dx.doi.org/10.2136/vzj2016.04.0033.

Stearns, M., Tindall, J., Cronin, G., Friedel, M., Bergquist, E., 2005. Effects of coal-bed methane discharge waters on the vegetation and soil ecosystem in Powder River Basin, Wyoming. Water Air Soil Pollut. 168, 33–57.

Vance, G.F., King, L.A., Ganjegunte, G.K., 2008. Soil and plant responses from land application of saline-sodic waters: implications of management. J. Environ. Qual. 37, S139–S148.

van Genuchten, M.Th., 1980. A closed-form equation for predicting the hydraulic conductivity of unsaturated soils. Soil Sci. Soc. Am. J. 44, 892–898.

Wesseling, J.G., Elbers, J.A., Kabat, P., van den Broek, B.J., 1991. SWATRE: Instructions for Input, Internal Note. Winand Staring Centre, Wageningen, The Netherlands.

White, N., Zelazny, L.W., 1986. Charge properties in soil colloids. In: Sparks, D.L. (Ed.), Soil Physical Chemistry. CRC Press, Boca Raton, FL.